Cell

Hypothalamic PNOC/NPY neurons constitute mediators of leptin-controlled energy homeostasis

Graphical abstract

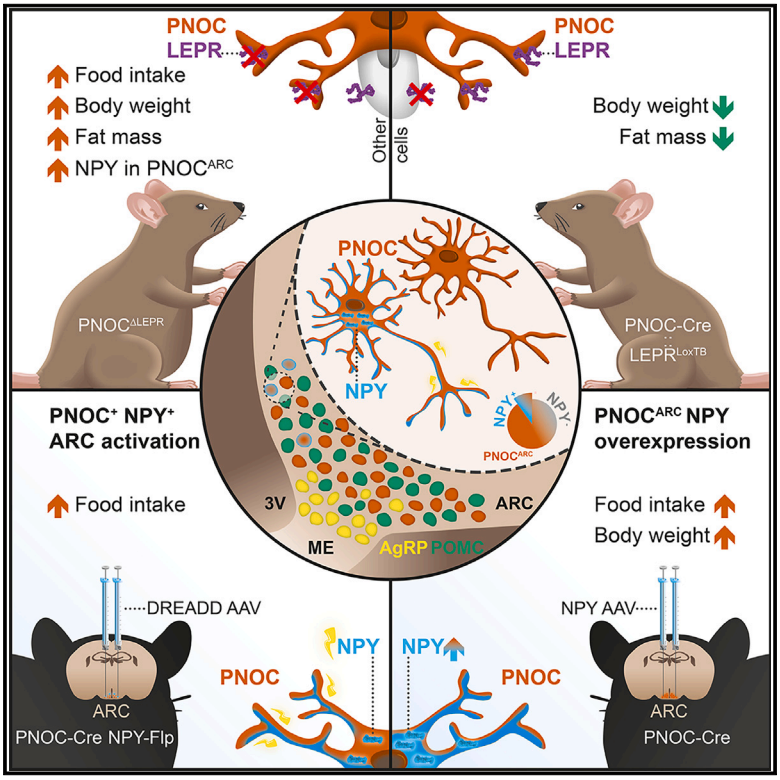

Highlights

- Loss of leptin receptors in PNOC^{ARC} neurons causes hyperphagia and obesity
- PNOC leptin receptor inactivation increases NPY expression in AgRP−/PNOC+ neurons
- Activation of NPY+/PNOC+ neurons induces feeding, similar to all PNOC^{ARC} neurons
- Overexpression of NPY in PNOC^{ARC} neurons induces hyperphagia and obesity

Authors

Marie H. Solheim, Sima Stroganov, Weiyi Chen, ..., F. Thomas Wunderlich, Lukas Steuernagel, Jens C. Brüning

Correspondence

bruening@sf.mpg.de

In brief

Activation of PNOC^{ARC} neurons promotes feeding. Here, Solheim et al. describe PNOC neurons in the murine ARC as mediators of leptin action in body weight maintenance. Moreover, they molecularly and functionally define a specific PNOC^{ARC} subtype, characterized by co-expression of PNOC and NPY, which is conserved in humans and regulates feeding in mice.

Solheim et al., 2025, Cell *188*, 1–17
June 26, 2025
https://doi.org/10.1016/j.cell.2025.04.001

Cell

CellPress
OPEN ACCESS

Article

Hypothalamic PNOC/NPY neurons constitute mediators of leptin-controlled energy homeostasis

Marie H. Solheim,[1] Sima Stroganov,[1] Weiyi Chen,[1] P. Sicilia Subagia,[1] Corinna A. Bauder,[1] Daria Wnuk-Lipinski,[1] Almudena Del Río-Martín,[1] Tamara Sotelo-Hitschfeld,[1] Cait A. Beddows,[2] Paul Klemm,[1] Garron T. Dodd,[2] Sofia Lundh,[3] Anna Secher,[3] F. Thomas Wunderlich,[1] Lukas Steuernagel,[1,4] and Jens C. Brüning[1,5,6,7,8,*]

[1]Department of Neuronal Control of Metabolism, Max Planck Institute for Metabolism Research, Cologne, Germany
[2]Department of Anatomy and Physiology, the University of Melbourne, Melbourne, VIC, Australia
[3]Global Drug Discovery, Novo Nordisk A/S, Måløv, Denmark
[4]Neurogenomics Group, Max Planck Institute for Metabolism Research, Cologne, Germany
[5]Policlinic for Endocrinology, Diabetes, and Preventive Medicine (PEDP), University Hospital Cologne, Cologne, Germany
[6]Excellence Cluster on Cellular Stress Responses in Aging Associated Diseases (CECAD) and Center of Molecular Medicine Cologne (CMMC), University of Cologne, Cologne, Germany
[7]National Center for Diabetes Research (DZD), Ingolstädter Landstrasse 1, 85764 Neuherberg, Germany
[8]Lead contact
*Correspondence: bruening@sf.mpg.de
https://doi.org/10.1016/j.cell.2025.04.001

SUMMARY

Leptin acts in the brain to suppress appetite, yet the responsible neurocircuitries underlying leptin's anorectic effect are incompletely defined. Prepronociceptin (PNOC)-expressing neurons mediate diet-induced hyperphagia and weight gain in mice. Here, we show that leptin regulates appetite and body weight via PNOC neurons, and that loss of leptin receptor (*Lepr*) expression in PNOC-expressing neurons in the arcuate nucleus of the hypothalamus (ARC) causes hyperphagia and obesity. Restoring *Lepr* expression in PNOC neurons on a *Lepr*-null obese background substantially reduces body weight. *Lepr* inactivation in PNOC neurons increases neuropeptide Y (*Npy*) expression in a subset of hypothalamic PNOC neurons that do not express agouti-related peptide (*Agrp*). Selective chemogenetic activation of PNOC/NPY neurons promotes feeding to the same extent as activating all PNOC^{ARC} neurons, and overexpression of *Npy* in PNOC^{ARC} neurons promotes hyperphagia and obesity. Thus, we introduce PNOC/NPY^{ARC} neurons as an additional critical mediator of leptin action and as a promising target for obesity therapeutics.

INTRODUCTION

Obesity and overnutrition represent global health burdens urgently demanding better treatment options.[1] For targeted therapeutics and proper management of the obesity pandemic, a better understanding of mechanisms controlling appetite and food consumption is warranted. An important regulator of food intake and body weight is leptin, a hormone secreted from the adipose tissue in direct proportion to fat mass.[2] Deficiency for leptin or its receptor (LEPR) provokes uncontrollable hunger and decreases energy expenditure (EE), resulting in severe obesity in mice and humans.[3,4] Leptin acts to suppress appetite by signaling via neurons that express *Lepr*.[5,6] In the arcuate nucleus of the hypothalamus (ARC), proopiomelanocortin (POMC)-expressing and agouti-related peptide (AgRP)/neuropeptide Y (NPY) co-expressing neurons play major roles in energy balance.[7] Despite this notion, leptin does not exert a major food-intake-regulatory function through direct action on POMC neurons of adult mice.[8,9] Prenatal ablation of LEPR in AgRP neurons results in only modest obesity, whereas ablation in adult animals induces considerable weight gain.[10,11] Interestingly, chronic activation of either ARC AgRP or non-AgRP GABAergic neurons both induce a similarly pronounced obese phenotype.[12] Thus, other molecularly undefined ARC GABAergic neurons contribute to the metabolism-regulatory function of leptin. We have recently identified GABAergic prepronociceptin (PNOC) neurons in the ARC to mediate high-fat-diet (HFD)-induced hyperphagia and weight gain in mice.[13] These PNOC^{ARC} neurons are a distinct but molecularly heterogeneous population of cells that directly inhibit POMC neurons.[13,14] Importantly, PNOC neurons are regulated by glucose, and a portion of the neurons have also been shown to be inhibited by leptin *ex vivo*.[13]

Here, we reveal that leptin exerts a substantial portion of its appetite- and body-weight-regulatory effects via hypothalamic PNOC-expressing neurons. We find that loss of *Lepr* expression in PNOC neurons causes obesity due to hyperphagia, but this effect is independent of *Pnoc* expression itself. Utilizing an unbiased RNA sequencing (RNA-seq) bacTRAP approach,

Please cite this article in press as: Solheim et al., Hypothalamic PNOC/NPY neurons constitute mediators of leptin-controlled energy homeostasis, Cell (2025), https://doi.org/10.1016/j.cell.2025.04.001

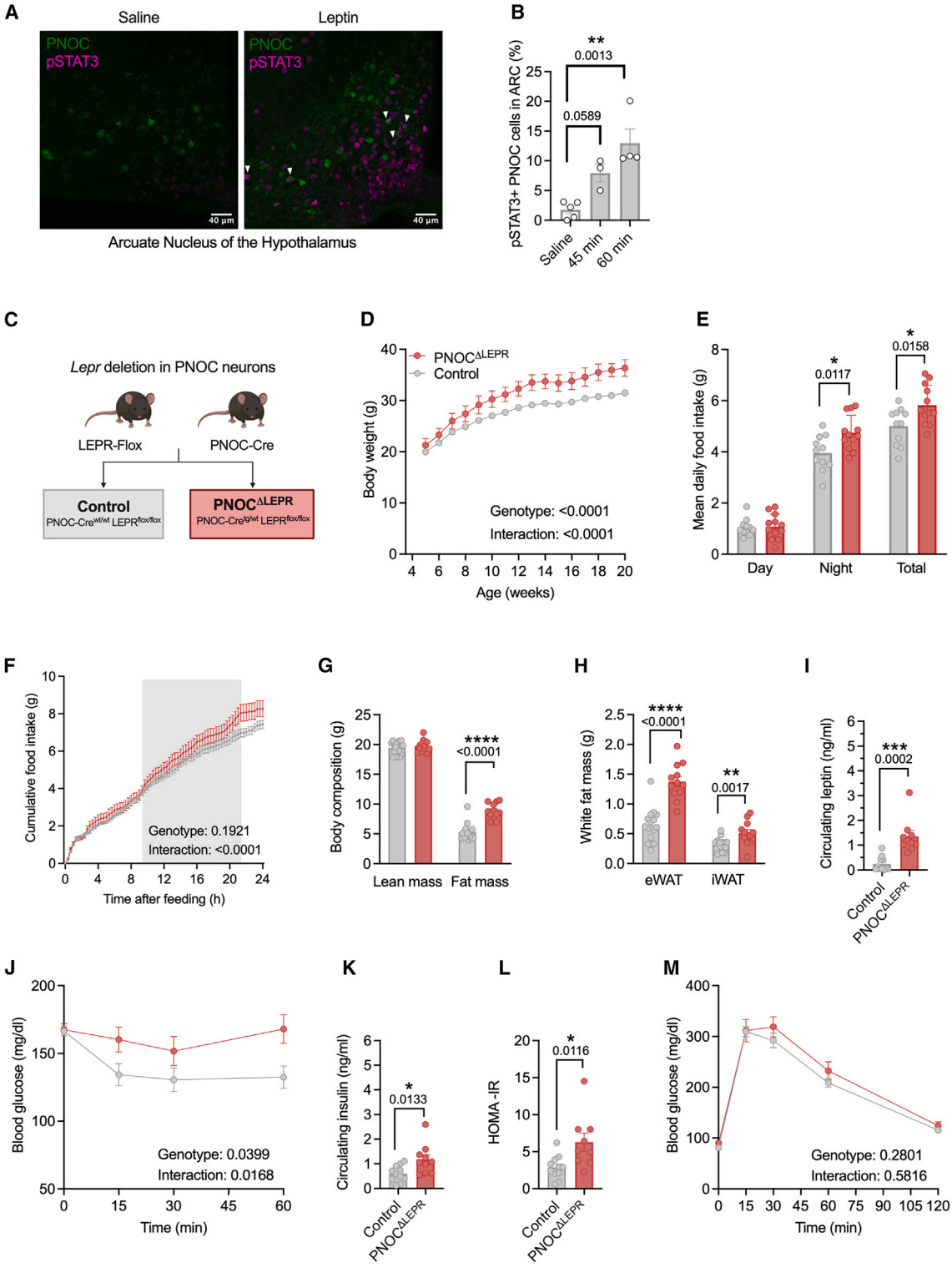

Figure 1. The absence of LEPRs in PNOC neurons results in increased food intake and fat mass

(A) Confocal images of brain sections showing immunoreactive pSTAT3 (magenta) and PNOC (EGFP, green) in the ARC of PNOC-EGFP mice fasted overnight (16 h) and sacrificed 60 min after an intraperitoneal (i.p.) injection of saline or leptin (6 mg/kg). Scale bars, 40 µm. Arrows indicate double staining.

(B) Quantification of percentage of pSTAT3-positive PNOC cells in the ARC, 45 and 60 min post leptin injections or 60 min post saline injections (n = 3–5/each group).

(legend continued on next page)

Please cite this article in press as: Solheim et al., Hypothalamic PNOC/NPY neurons constitute mediators of leptin-controlled energy homeostasis, Cell (2025), https://doi.org/10.1016/j.cell.2025.04.001

we find that loss of LEPRs in PNOC neurons leads to elevated *Npy* expression in *Agrp*-negative PNOC neurons, and we further identify a population of PNOC neurons in the ARC that do not express *Agrp* but co-express *Npy*. Interestingly, these neurons, to a large extent, also co-express *Lepr*, their selective chemogenetic activation strongly promotes food intake, and they are conserved in the human hypothalamus. Moreover, adeno-associated virus (AAV)-mediated expression of *Npy* in PNOC neurons, but not in AgRP neurons, in the ARC promotes hyperphagia and obesity development. Taken together, we introduce the PNOC/NPY/LEPR neurons as a mediator of leptin action with promising prospects for targeted obesity therapeutics.

RESULTS

Leptin action in PNOC neurons is limited to those in the ARC

PNOC-expressing neurons are widely distributed across the mouse brain, including regions of the bed nucleus of the stria terminalis (BNST), central amygdala (CeA), and hypothalamic nuclei.[13–15] Nevertheless, using PNOC-EGFP mice, we found that leptin-induced pSTAT3 signaling in PNOC neurons is largely limited to those located in the ARC. Up to 13% of EGFP-positive $PNOC^{ARC}$ cells exhibited pSTAT3 immunoreactivity 45–60 min following peripheral leptin administration (Figures 1A and 1B), whereas very few to no pSTAT3-positive PNOC cells were observed in the amygdala (Amy), BNST, or other PNOC-expressing regions, including the lateral tuberal nucleus, the dorsomedial hypothalamic nucleus (DMH), and the nucleus tractus solitarius (NTS) (Figures S1A–S1C). These observations are consistent with our previous studies where specific optogenetic activation of $PNOC^{ARC}$ neurons promotes feeding and that they, *ex vivo*, are in part inhibited by leptin.[13]

Leptin receptors in PNOC neurons are required for the control of body weight and food intake

To determine the functional role of LEPRs in PNOC neurons, we generated mice lacking LEPRs in all PNOC-expressing neurons ($PNOC^{\Delta LEPR}$) (Figures 1C, S1D, and S1E). These mice displayed considerably higher body weight compared with control littermates shortly after weaning (Figure 1D). At 8 weeks of age $PNOC^{\Delta LEPR}$ mice weighed 11.8% more than controls (2.89 g ± 0.55 SEM difference, $p \leq 0.0001$), and the difference reached 15.5% (4.87 g ± 0.52 SEM difference, $p \leq 0.0001$) at 20 weeks of age. The higher body weight was accompanied by hyperphagia, with a ~10% increase in daily food intake and a prolonged re-feeding period after a 16-h fast (Figures 1E and 1F). This obese phenotype was observed despite no changes in respiratory exchange ratio (RER), EE, or locomotion (Figures S1F–S1H). In addition, $PNOC^{\Delta LEPR}$ mice showed significantly increased adiposity, with a larger total fat mass (3.57 g ± 0.50 SEM difference, $p \leq 0.0001$) by micro-computed tomography (uCT) at 15 weeks of age, increased *post mortem* white adipose fat tissue weights (Figures 1G and 1H), and enlarged adipocytes consistent with metabolic dysfunction (Figures S1I–S1L). As a consequence, circulating leptin levels were ~2.5-fold higher compared with control animals (Figure 1I). Alongside the obese phenotype, $PNOC^{\Delta LEPR}$ mice displayed insulin resistance by insulin tolerance tests, elevated circulating insulin levels, and elevated HOMA-IR indices (Figures 1J–1L). Glucose tolerance remained normal (Figure 1M).

Restoring leptin receptor expression selectively in PNOC neurons reduces body weight in otherwise leptin-receptor-deficient mice

To examine the effect of restoring *Lepr* expression specifically in PNOC cells on a *Lepr*-null background, we crossed PNOC-Cre mice to $LEPR^{LoxTB}$ mice[16] (Figure 2A). Re-introducing LEPRs in PNOC-expressing cells alone (PNOC-Cre::$LEPR^{LoxTB}$) generated mice that were already visually leaner and had a significantly lower body weight by 15.7% (9.65 g ± SEM 1.98, $p \leq 0.0006$) compared with $LEPR^{LoxTB}$ mice (Figures 2B–2D). In fact, ~30% of the weight gain observed in *Lepr*-null $LEPR^{LoxTB}$ mice compared with control mice was attributed to the lack of LEPR action in PNOC neurons. Upon uCT analysis, the PNOC-Cre::$LEPR^{LoxTB}$ also exhibit a 36.2% (24.56 g ± SEM 1.44 vs. 38.55 ± SEM 1.37 in $LEPR^{LoxTB}$, $p \leq 0.0001$) reduction in fat mass compared with the $LEPR^{LoxTB}$ animals (Figure 2E).

As expected, brains from $LEPR^{LoxTB}$ mice showed a complete absence of leptin-evoked pSTAT3 immunoreactivity, whereas brains extracted from PNOC-Cre::$LEPR^{LoxTB}$ showed some degree of pSTAT3-positive cells (~45% of control mice) in the ARC (Figures 2F and 2G). The location of the pSTAT3-positive cells was consistent with that of $PNOC^{ARC}$ neurons, distinct from the anatomical localization of AgRP cells (Figure 2F). In contrast, the pSTAT3 signal in the ARC from lean control animals with intact global *Lepr* expression included the localization of AgRP neurons and showed a significantly higher number of pSTAT3-positive cells than that of PNOC-Cre::$LEPR^{LOXTB}$ animals (Figures 2F and 2G).

Together, we find that leptin action on PNOC neurons is required to maintain normal body weight. Their action profoundly regulates food intake, even in the absence of other LEPR populations, emphasizing their substantial regulatory role in food intake and body weight.

(C) Schematic of the knockout strategy used to inactivate *Lepr* in PNOC cells.
(D) Weekly body weight progression in male LEPR-Flox control (gray) and $PNOC^{\Delta LEPR}$ mice (red) measured over the indicated time course.
(E and F) (E) Mean daily food intake, shown as average of 2 consecutive days, and (F) cumulative food intake following a 16-h fasting period at 15 weeks of age (gray area indicates dark/night phase).
(G–I) (G) uCT analysis of lean and fat mass, (H) *post mortem* dissected fat mass at 20 weeks of age and (I) circulating fasted leptin levels.
(J–L) (J) Insulin tolerance test, (K) circulating fasted insulin levels, and (L) HOMA-IR calculations at 12 weeks of age.
(M) Glucose tolerance tests performed at 13 weeks of age. Data are represented as mean ± SEM. Male animals, $n = 12–17$, with the exception of food intake ($n = 12$ vs. 12) and leptin/insulin level ($n = 11$ vs. 9). p values calculated using one-way ANOVA followed by Tukey's multiple comparison test (B), two-tailed unpaired Student's t test (E, G–I, K, and L), or two-way RM ANOVA (D, F, J, and M). *p ≤ 0.05; **p ≤ 0.01; ***p ≤ 0.001; ****p ≤ 0.0001.
See also Figures S1, S2, and S4.

Please cite this article in press as: Solheim et al., Hypothalamic PNOC/NPY neurons constitute mediators of leptin-controlled energy homeostasis, Cell (2025), https://doi.org/10.1016/j.cell.2025.04.001

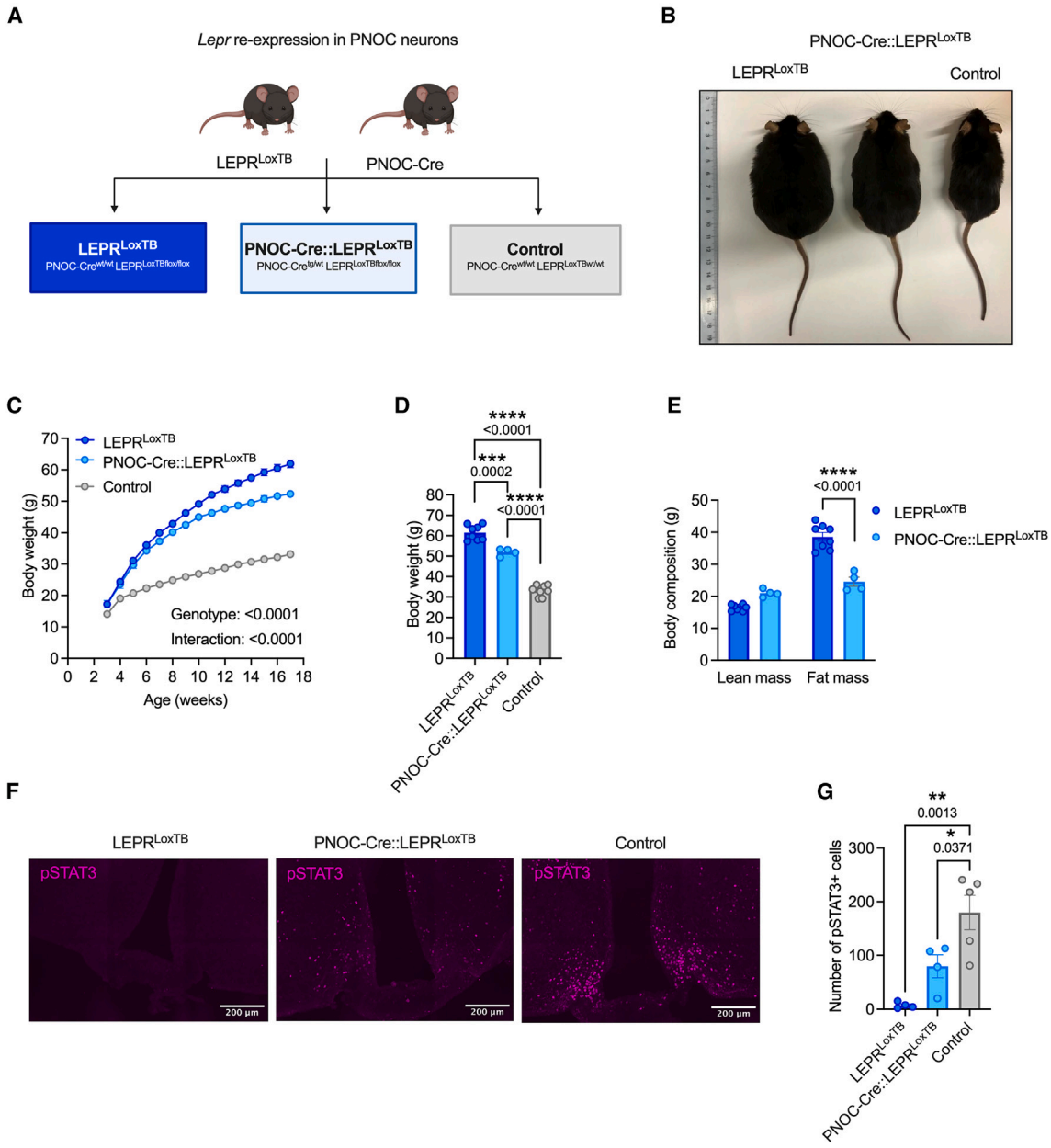

Figure 2. Restoring leptin action selectively in PNOC neurons reduces body weight and food intake in LEPR-deficient mice

(A) Schematic of the study groups for examining reactivation of *Lepr* in PNOC cells in otherwise *Lepr*-null mice. LEPR^{LoxTB} mice were bred with PNOC-Cre mice, creating LEPR^{LoxTB}, PNOC-Cre::LEPR^{LoxTB}, and control mice.

(B) Photo illustrating visual body weight differences.

(C) Weekly body weight progression in male LEPR^{LoxTB} (dark blue), PNOC-Cre::LEPR^{LoxTB} (light blue), and control mice (gray) (n = 4–8).

(D and E) (D) Body weights at 16 weeks of age and (E) uCT analysis of lean and fat mass.

(F and G) (F) Representative images of immunoreactive pSTAT3 (magenta) in each group, 1 h post leptin injection in mice after a 16-h fasting period and (G) quantified number of pSTAT3+ cells in the ARC. Scale bars, 200 µm. Data are represented as mean ± SEM. p values calculated using two-way RM ANOVA (C), one-way ANOVA followed by Tukey's multiple comparison test (D and G), or two-tailed unpaired Student's t test (E). *p ≤ 0.05; **p ≤ 0.01; ****p ≤ 0.0001.

Leptin action specifically in PNOC neurons of the ARC controls body weight and food intake

Next, we locally ablated *Lepr* expression in PNOC^{ARC} neurons using a CRISPR-Cas9 approach. Specifically, we bred PNOC-Cre animals with Rosa26-LSL-Cas9-GFP knockin mice,[17] leading to animals that exclusively express the *Cas9* endonuclease in PNOC neurons, and injected bilaterally into the ARC AAVs, allowing for expression of guide RNAs targeting the mouse *Lepr* locus (Figures S2A and S2B). To confirm PNOC^{ARC}-specific inactivation of LEPRs, we amplified the genome-edited region of the *Lepr*

Please cite this article in press as: Solheim et al., Hypothalamic PNOC/NPY neurons constitute mediators of leptin-controlled energy homeostasis, Cell (2025), https://doi.org/10.1016/j.cell.2025.04.001

CellPress
OPEN ACCESS

A

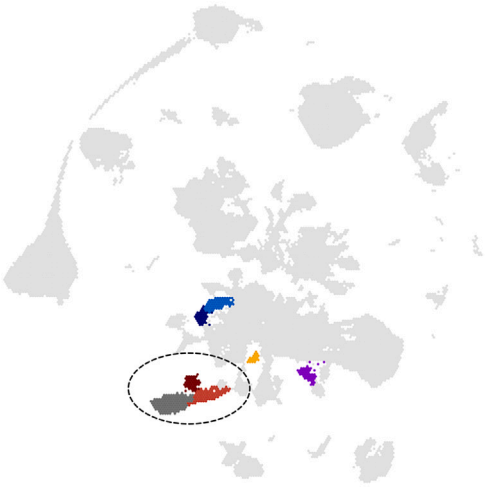

B

PNOC^ARC Clusters	Sn Avg exp PNOC	Sn % of all PNOC+	ISH % of all PNOC+	ISH % LEPR+
Crabp1 — Cluster 1 (Htr3b) C185-103: Vgll3.Tbx3.GABA-1	1.08	10.88	10.42	29.13
Crabp1 — Cluster 2 (Tmem215) C185-104: Sy64.Tbx3.GABA-1	0.72	10.90	35.65 / N/A	17.48 / N/A
Satb2 — Cluster 3 (Nfix/Glp1r) C185-127: Nfix.Satb2.GABA-6	0.99	7.49	8.28	1.49
Otp — Cluster 4 (Chst9/Nts) C185-119: Nts.Sst.GABA-4	0.79	3.61	9.71	27.19
Otp / Sst — Cluster 5 (Sst/Unc13c) C185-118: Otp.Sst.GABA-4	0.73	12.31	N/A	N/A
Otp / Sst / Npy — Cluster 6 (Sst/Npy) C185-117: Npy.Sst.GABA-4	1.78	16.52	41.41 / 4.46	31.79 / 78.13
Otp / Npy — Cluster 7 (Agrp/Npy) C66-46: Agrp.GABA-4	0.27	8.75	5.68	53.96
Other ARC	0.25	29.53		

C

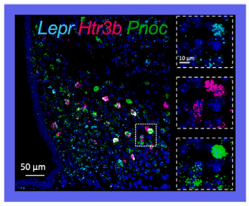

D

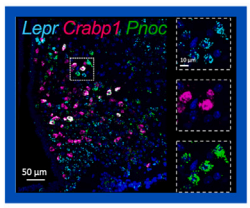

E

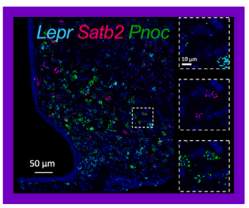

F

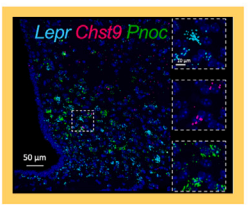

G

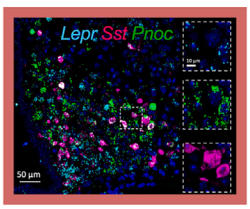

H

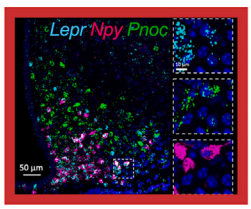

I

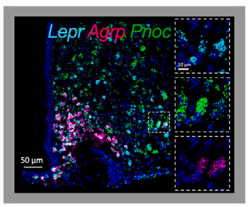

J

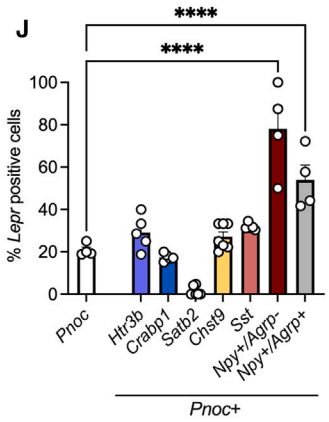

K

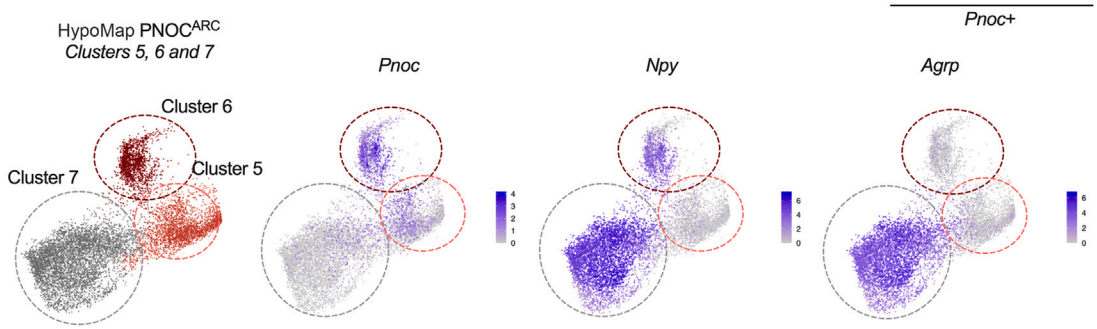

(legend on next page)

gene using a PCR strategy where primers flank the edited region. In tail, Amy, and hypothalamus biopsies of control and Cas9+ animals, we detect a full-length unedited genomic *Lepr* band covering exon 7–9, at 3,480 bp, whereas the shorter 307-bp band, resulting from genome editing, was only observed in hypothalamic samples from Cas9+ animals (Figures S2C and S2D).

Importantly, CRISPR-mediated deletion of LEPRs in PNOC^{ARC} neurons caused obesity, with a 2-fold increase in weight gain post injection as well as significantly larger fat mass (Figures S2E and S2F). It also led to a ~13% increase in food intake and a slightly higher RER and EE (Figures S2G–S2I).

Collectively, we define a functional role for leptin action on PNOC neurons in the ARC and find that ablating LEPRs in a PNOC^{ARC}-specific manner causes hyperphagia and obesity similar to what is observed upon ablation of LEPRs in all PNOC neurons.

Hyperphagia and obesity development upon leptin receptor deletion in PNOC-expressing cells is independent of PNOC expression

Aside from a shared expression of PNOC, these neurons are diverse and heterogeneous in their molecular signature, and we have previously shown that GABA release from PNOC^{ARC} neurons can inhibit food intake suppressing POMC neurons.[13] It has also previously been shown that nociceptin can inhibit POMC neuronal activity.[18] Given that leptin can suppress the activity of PNOC^{ARC} neurons, leptin-evoked suppression of feeding via PNOC neurons might also involve reduced nociceptin release from these cells. To directly address this question, we created PNOC$^{\Delta LEPR\Delta PNOC}$ mice (Figure S3A). Ablating LEPRs from PNOC cells and simultaneously inactivating *Pnoc* expression resulted in obesity to the same degree as those expressing *Pnoc*, indicating that nociceptin expression does not contribute to leptin's ability to regulate food intake control via PNOC neurons (Figures S3B–S3D). Similarly, abrogated nociceptin production in PNOC cells had no impact on insulin tolerance or glucose sensitivity in mice, with or without LEPRs (Figures S3E and S3F). This is consistent with our recent observation that nociceptin expression in PNOC^{ARC} neurons is dispensable for the food intake stimulatory effect of their optogenetic activation.[19]

PNOC neurons in the ARC comprise seven molecularly distinct neuron subtypes

Recently, we have generated HypoMap as a unified single-cell and nucleus gene expression atlas of the murine hypothalamus.[14] Employing HypoMap, we identified seven candidate PNOC neuronal populations that are predicted to reside in or close to the ARC, all of which are GABAergic. They comprise two cellular retinoic-acid-binding protein (*Crabp1*)-expressing populations, expressing either the serotonin 5-hydroxytryptamine receptor 3b (*Htr3b*) (cluster #1) or the transmembrane protein 215 (*Tmem215*) (cluster #2), one special AT-rich sequence-binding protein 2 (*Satb2*)-expressing group of PNOC neurons (cluster #3), and four orthopedia homeobox (*Otp*)-expressing populations. These *Otp*-expressing clusters are characterized by the co-expression of *Chst9* (cluster #4), somatostatin (*Sst*) and *Unc13* (cluster #5), Sst and *Npy* (cluster #6), or *Npy* and *Agrp* (cluster #7) (Figures 3A and 3B). Consistent with the analysis of single-cell and nucleus sequencing data (from here, collectively referred to as sn sequencing) from HypoMap, *in situ* hybridization experiments revealed that *Crabp1*-expressing clusters #1 and #2 account for ~35% of all PNOC^{ARC} neurons, and cluster #1, characterized by the co-expression of *Crabp1* and *Htr3b*, accounts for ~10% of PNOC^{ARC} neurons (Figures 3B–3I). *Satb2*-positive cluster #3 cells account for ~8% of PNOC^{ARC} neurons, whereas *Otp*-expressing clusters #4–7 account for ~56% of PNOC^{ARC} neurons; here, the majority (~41% of all PNOC^{ARC} neurons) express *Sst* (clusters #5 and #6), of which a minor proportion expresses *Npy*, but not *Agrp* (~4% of all PNOC^{ARC} cells), which characterizes the PNOC neurons in cluster #6. Finally, cells in cluster #7, characterized by *Npy* and *Agrp* co-expression, comprise ~5% of all PNOC^{ARC} neurons (Figures 3B–3I). In turn, *Pnoc* expression is detected in 4% of AgRP neurons (RNAscope-based *in situ* hybridization, data not shown), but, of note, *Pnoc* is expressed at a level that is 15 times lower in cluster #7 compared with cluster #6 cells, which exhibit the highest level of *Pnoc* expression among all PNOC^{ARC} neurons (Figure 3B).

Next, we assessed the relative proportion of cells in each of these PNOC^{ARC} clusters that expresses *Lepr* using RNAscope-based *in situ* hybridization. Consistent with the proportion of PNOC^{ARC} neurons responding to leptin by increased STAT3 phosphorylation (Figures 1A and 1B), ~18% of the overall PNOC^{ARC} population expressed *Lepr* (Figure 3J). Cells in cluster #6 (PNOC+/NPY+/AgRP− neurons) exhibited the highest degree of *Lepr* expression with 78%, followed by cluster #7 (PNOC+/NPY+/AgRP+) neurons with 54% *Lepr*-positive cells, CRABP1+/HTR3B+ cells in cluster #1 with 29% of *Lepr*-positive cells, and CHST9+ cells in cluster #4 with 27% *Lepr*-expressing cells, whereas the remaining clusters #2, #3, and #5 expressed

Figure 3. PNOC ARC neurons represent molecularly heterogeneous cell types

(A) Uniform manifold approximation and projection (UMAP) for dimension reduction of the full murine HypoMap dataset to highlight PNOC^{ARC} clusters in different colors.

(B) Table with overview of seven PNOC^{ARC} clusters defined in this study. Genes used to mark clusters in *in situ* hybridization (ISH) validation are highlighted as bold and underlined. Columns from left to right: (1) cluster number and name, including HypoMap identifier and prominent marker genes; (2) sn avg exp PNOC: average *Pnoc* expression in the individual PNOC-expressing HypoMap clusters; (3) sn% of all PNOC+: percent of all PNOC-expressing cells in ARC clusters of HypoMap; (4) ISH% of all PNOC+: percent of cells expressing ISH marker for cluster of all *Pnoc*-expressing cells in ARC based on ISH analysis; and (5) ISH% of all LEPR: percent of cells expressing *Lepr* within ISH cluster (*Pnoc*+ Marker).

(C–I) Representative images of ISH for marker genes of PNOC clusters as defined in (B) together with *Pnoc* and *Lepr*. Scale bars 40 μm and 20 μm (zoom).

(J) Quantification of percent *Lepr*+ cells in each *Pnoc*+-selected marker-gene-expressing cell cluster ($n = 2$ sections of 4–7 mice) and one-way ANOVA followed by Dunnett's multiple comparison test, comparing each cluster to the all *Pnoc* control groups, presented as mean ± SEM. ****$p \leq 0.0001$.

(K) Detailed UMAP of HypoMap clusters #5–7, including SST and AGRP neurons. UMAP plots to the right show the sn sequencing log-normalized expression of *Pnoc*, *Npy*, and *Agrp*, respectively.

See also Figures S3 and S7.

Please cite this article in press as: Solheim et al., Hypothalamic PNOC/NPY neurons constitute mediators of leptin-controlled energy homeostasis, Cell (2025), https://doi.org/10.1016/j.cell.2025.04.001

the *Lepr* at lower percentages than the overall PNOC^{ARC} population (Figures 3B–3J). A detailed uniform manifold approximation and projection (UMAP) of HypoMap clusters #5–7 and the sn sequencing log-normalized expression of *Pnoc*, *Npy*, and *Agrp* further reveal their unique gene expression profiles (Figure 3K).

Thus, PNOC^{ARC} neurons are highly heterogeneous and contain distinct subsets of leptin-sensitive cells, which potentially contribute to the food-intake-regulatory function exerted by leptin via the regulation of PNOC^{ARC} cells.

Leptin receptor expression in HTR3B-expressing ARC neurons is dispensable for energy homeostasis

Because an enrichment for *Lepr* expression was observed in *Htr3b*-expressing cluster #1 PNOC^{ARC} neurons, we first investigated the functional role of *Lepr* expression specifically in this PNOC population. To this end, we created HTR3B-Cre mice and further confirmed HTR3B-neuron-restricted expression by Cre-dependent L10a-GFP expression[9] (Figure S3G). *In situ* hybridization revealed that 88.5% of the *Htr3b*-expressing cells co-expressed *L10a-GFP* (Figure S3H). Next, we generated mice lacking LEPRs in the HTR3B-expressing neurons (HTR3B$^{\Delta LEPR}$) (Figure S3I); however, we observed no difference in body weight over a time span of 20 weeks (Figure S3J) and no differences in feeding behavior (Figures S3K and S3L) or body composition measured by uCT (Figure S3M).

Leptin receptor deletion in PNOC-expressing cells increases *Npy* expression in PNOC^{ARC} neurons

To potentially identify the PNOC^{ARC} neuron cluster(s) through which *Lepr* ablation promotes hyperphagia and obesity development, we compared the translational profiles of LEPR-proficient and -deficient PNOC neurons. We crossed the PNOC-Cre (control) and PNOC$^{\Delta LEPR}$ animals with ROSA-STOP-L10a-bacTRAP mice,[9] allowing for Cre-dependent expression of the fusion protein of the ribosomal protein L10a tagged with GFP specifically in PNOC neurons (Figures 4A and S4A). *In situ* hybridization experiments further confirmed that 98% of the *Pnoc*-expressing cells co-expressed *L10a-GFP* (Figure S4B). From L10a-bacTRAP animals, we harvested hypothalamic samples and used an anti-GFP antibody to precipitate ribosomes of PNOC neurons. RNA-seq of mRNA associated with immunopurified ribosomes from PNOC neurons yielded a detailed translational profile of hypothalamic PNOC neurons, and analyzing exon-spanning reads in the *Lepr* gene also confirmed the efficient exclusion of exon 1 from the targeted allele of PNOC$^{\Delta LEPR}$ mice (Figure S4C).

We first evaluated total input samples vs. immunoprecipitated (IP) samples and found a clear separation by principal-component analysis (PCA) and a clear separation between the two genotypes (Figure S4D). We then defined genes that were differentially upregulated between IP and input samples in either genotype as PNOC-neuron-enriched genes (3,550 total, $\log_2$FC > 0.5, adjusted p value < 0.05). When comparing the IP samples of control and PNOC$^{\Delta LEPR}$ mice, we found a total of 1,052 significantly up- or downregulated genes (adjusted p value < 0.05), 236 of which exhibited enriched expression in PNOC neurons (Figures 4B, S4E, and S4F). Gene Ontology (GO) enrichment analysis identified biological processes, such as regulation of hormone secretion and neuropeptide signaling pathways, oxidative phosphorylation, and aerobic respiration, as the top enriched differentially regulated biological processes (Figures S4G and S4H). Remarkably, among the PNOC-neuron-enriched, differentially expressed genes, *Npy* stood out as one of the top upregulated genes in PNOC$^{\Delta LEPR}$ mice compared with control (Figures 4B and 4C), which also represented the top hit in the GO term "neuropeptide signaling."

The signatures of PNOC bacTRAP sequencing experiments represent a mixture of the heterogeneous PNOC populations in the hypothalamus. To further delineate which of the seven identified PNOC^{ARC} neuronal populations could be responsible for the observed effect on food intake, we compared bacTRAP and sn sequencing data. The top five marker genes of each PNOC^{ARC} population in the sn sequencing data of HypoMap (Figures 3A and 3B) are depicted in Figure 4D, demonstrating their distinct molecular identities. Comparing the $\log_2$-fold changes of these marker genes between the IP samples of PNOC$^{\Delta LEPR}$ and control animals revealed that the pull-down enriched for the *Crabp1*- and *Sst*-expressing populations (Figure 4E). Strikingly, increased *Npy* expression is restricted to one of the *Sst*-expressing PNOC populations, which is distinct from AgRP neurons, indicating that the LEPR deficiency specifically had an effect in this cell type (cluster #6 of PNOC^{ARC} neurons).

Activating PNOC+/NPY+ neurons in the ARC robustly stimulates food intake in mice

NPY in the ARC is an important regulator of feeding; however, how NPY promotes feeding under obese conditions is not fully defined. The upregulation of *Npy* in our PNOC$^{\Delta LEPR}$ model could potentially explain their hyperphagia. Our detailed *in situ*-hybridization-based sub-clustering of PNOC^{ARC} populations (Figure 3) has revealed that two PNOC-expressing cell clusters in the ARC also express *Npy*, i.e., cluster #6 (PNOC+/NPY+/AgRP− neurons) and cluster #7 (PNOC+/NPY+/AgRP+ cells). These clusters also showed the highest levels of *Lepr* expression.

To determine the specific contribution of the PNOC+/NPY+ neuronal population to the control of feeding, we used intersectional Cre/Flp-dependent expression of hM3D(Gq) Designer Receptors Activated Only by Designer Drugs (DREADDs), allowing for targeting cell populations expressing either only Cre and Flp, Cre but not Flp, or Flp but not Cre (Figure 5A). Combining AAVs and crossing PNOC-Cre to NPY-Flp mice led to the generation of six different groups of animals expressing the DREADD receptor hM3Dq, allowing for clozapine-N-oxide (CNO)-induced activation of (1) no ARC cells, (2) all NPY+ neurons, (3) NPY+/PNOC- neurons, (4) all PNOC+ neurons, (5) PNOC+/NPY+ neurons, and (6) PNOC+/NPY− neurons (Figures 5A and 5B).

Activation of all NPY+ cells resulted in the largest food intake (1.35 g) 4 h after CNO injection compared with mice that did not express hM3Dq (0.24 g) (Figure 5C). Selective activation of NPY+/PNOC− cells markedly induced feeding (0.95 g); however, this effect was slightly—although not significantly—reduced compared with mice where all NPY+ cells were activated. Consistent with our previous optogenetic stimulation of PNOC^{ARC} neurons, activation of all PNOC+ cells robustly increased food intake (0.74 g), although to lesser extent than

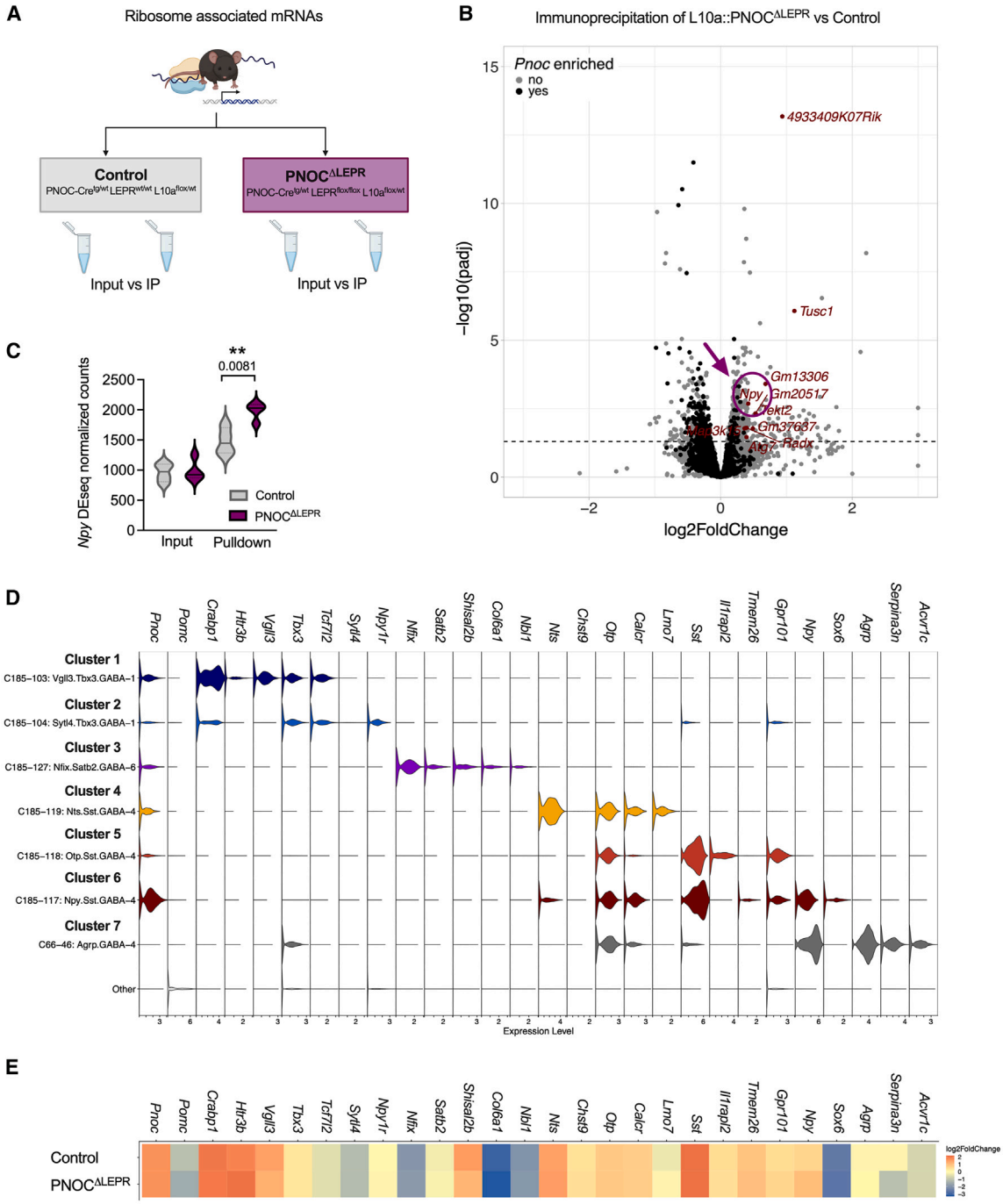

Figure 4. NPY expression is elevated in PNOC$^{\Delta LEPR}$ mice

(A) Schematic of mouse line allowing for Cre-dependent expression of the ribosomal protein L10a fused to GFP in Cre-expressing PNOC neurons of control (gray) and PNOC$^{\Delta LEPR}$ mice (purple). Hypothalamic sections were dissected and subjected to bacTRAP-based ribosomal profiling.

(B) Volcano plot of up- and downregulated genes in IP samples, highlighting 3,550 *Pnoc*-enriched genes in black. The dotted line marks an adjusted *p* value of 0.05.

(C) Extracted expression values of *Npy* in IP samples of control and PNOC$^{\Delta LEPR}$ samples, presented as DEseq-size factor-normalized counts, presented as mean ± SEM, and *p* values calculated using one-way ANOVA followed by Tukey's multiple comparison test.

(D) Violin plots of top five marker genes for the PNOC ARC clusters #1–7, showing distribution of log-normalized gene expression in cells of those populations using the reference atlas HypoMap.

(E) Log_2-fold changes of top five marker genes in (D) between IP and input samples of either control and PNOC$^{\Delta LEPR}$ mice, showing which of the populations are enriched in the bacTRAP IP data.

See also Figure S4.

Please cite this article in press as: Solheim et al., Hypothalamic PNOC/NPY neurons constitute mediators of leptin-controlled energy homeostasis, Cell (2025), https://doi.org/10.1016/j.cell.2025.04.001

CellPress
OPEN ACCESS

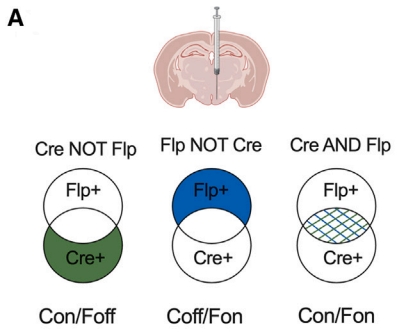

B

	Experimental setup							
CNO activation	No cells			All NPY+	NPY+/PNOC-	All PNOC+	PNOC+/NPY+	PNOC+/NPY-
Mouse Genotype	Cre+/Flp- or wt/wt	Cre-/Flp+ or wt/wt	Cre+/Flp-, Cre-/Flp+ or wt/wt	Cre-/Flp+	Cre+/Flp+	Cre+/Flp-	Cre+/Flp+	Cre+/Flp+
AAV	Coff/Fon	Con/Foff	Con/Fon	Coff/Fon	Coff/Fon	Con/Foff	Con/Fon	Con/Foff

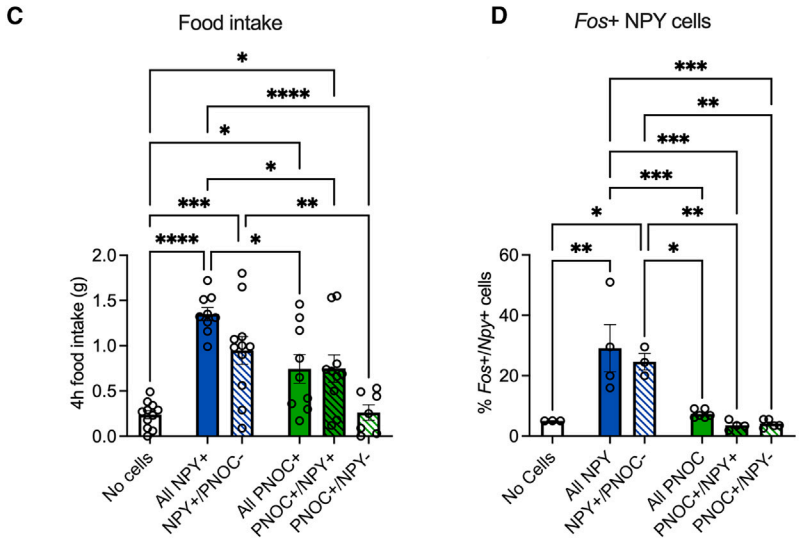

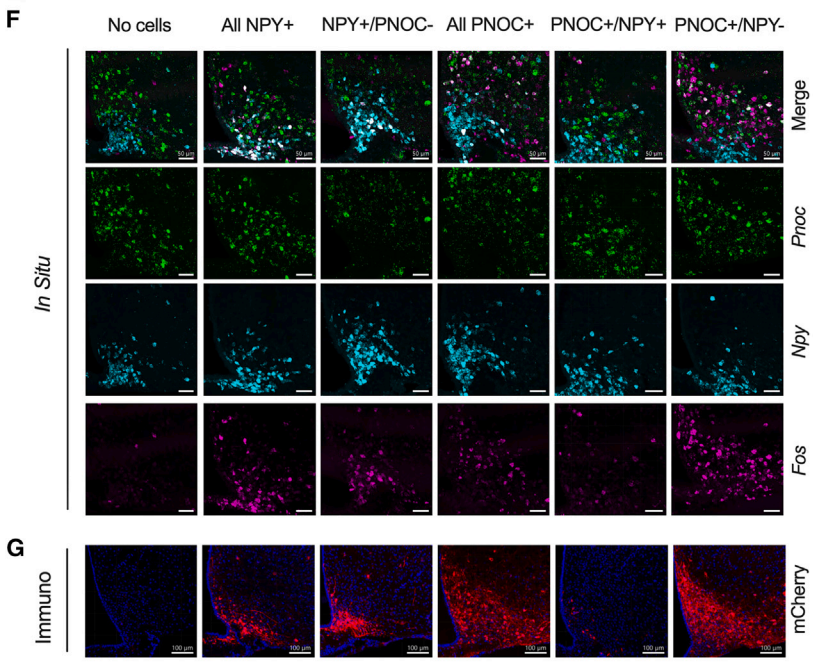

(legend on next page)

Please cite this article in press as: Solheim et al., Hypothalamic PNOC/NPY neurons constitute mediators of leptin-controlled energy homeostasis, Cell (2025), https://doi.org/10.1016/j.cell.2025.04.001

activating all NPY neurons (Figure 5C). Strikingly, selectively activating only PNOC+/NPY+ neurons, which account for 10% of the global PNOC^{ARC} population, stimulated food intake to the same magnitude as activating all PNOC^{ARC} neurons (0.75 g). In contrast, activating the remaining majority of PNOC^{ARC} neurons, which do not co-express *Npy*, failed to promote food intake (0.26 g) (Figure 5C). Treatment with saline in either group did not affect food intake (Figure S5A).

To investigate the cell-type-specific targeting and activation in the different groups, we injected the animals with CNO (1 mg/kg) 1 h before sacrifice and performed *in situ* hybridization experiments with probes directed to the mRNAs of *Pnoc*, *Npy*, and *Fos*. Mice expressing hM3Dq in all NPY neurons or in all NPY+/PNOC− neurons exhibited a robust, comparable increase in the proportion of *Fos*+ *Npy*-expressing neurons (Figures 5D and 5F). In contrast, and consistent with the overall contributions of PNOC+ neurons to NPY+ neurons in the ARC, neither of the groups that expressed hM3Dq in PNOC neurons increased the proportion of *Fos*+ *Npy*-expressing neurons (Figures 5D and 5F). Similarly, activating either all NPY+ neurons or NPY+/PNOC− neurons did not increase the proportion of *Fos*+ *Pnoc*-expressing neurons (Figures 5E and 5F). In contrast activating all PNOC+ neurons or PNOC+/NPY− neurons clearly increased the proportion of *Fos*+ *Pnoc* neurons (Figures 5E and 5F). Immunostaining directed at mCherry confirms the expected anatomical localization of the targeted cells in each group (Figure 5G). Further analysis of mice, where only PNOC+/NPY+ neurons were targeted, revealed a clear increase in the proportion of *Fos*+ cells within this specific subpopulation, with 58% of PNOC+/NPY+ neurons exhibiting *Fos* expression upon CNO stimulation (Figure S5B). Because PNOC+/NPY+ cells comprise cluster #6 (PNOC+/NPY+/AgRP− neurons) and cluster #7 (PNOC+/NPY+/AgRP+ cells), we next investigated to what extent cluster #6 and cluster #7 cells had been targeted via Cre/Flp-dependent targeting. To this end, we performed an *in situ* hybridization experiment in PNOC-Cre::NPY-Flp mice that had been given the CreON/FlpON AAV, with probes directed against *Pnoc, AgRP*, and *Fos*. This revealed that, upon CNO injection, the majority of *Fos*+ *Pnoc* cells were cluster# 6, *Agrp*− cells (84.34%), and only 15.66% were cluster #7 neurons, *Agrp*+ cells (Figure S5C). This effect may arise from the 15-times-higher expression level of *Pnoc* and, thus Cre, in cluster #6 compared with cluster #7 cells (Figure 3), thus potentially favoring more efficient Cre-dependent recombination in this cell type. Collectively, predominant activation of cluster #6 neurons accounts for the food intake stimulatory effect of activating all PNOC^{ARC} cells.

The PNOC/NPY subpopulation is inhibited upon food intake

In a recent study employing single-cell Ca^{2+} imaging *in vivo*, we revealed that PNOC^{ARC} neurons, similar to their molecular heterogeneity, also exhibit heterogeneous responses to feeding-state transitions. Although some PNOC neurons become activated upon re-feeding or intragastric calorie delivery, a portion do not respond, whereas a smaller subpopulation is profoundly inhibited. Of note, although the activated or non-responding PNOC neurons do not alter their responses after HFD feeding, the inhibited PNOC neurons become disinhibited.[19] To further investigate how the PNOC/NPY subpopulation responds to feeding transitions, we expressed a cytosolic calcium sensor GCaMP6s in a CreON/FlpON manner in PNOC-Cre::NPY-Flp mice and implanted a gradient-index (GRIN) lens directly above the ARC (Figures S5D–S5F). Remarkably, recordings of single PNOC/NPY neurons showed a much more uniform regulatory pattern than the full PNOC^{ARC} population. Re-feeding, following a 16-h overnight fast, rapidly inhibited 73.1% of the neurons (down), whereas only 20.8% of the neurons were activated (up). 6.1% were classified as non-responders (Figures S5G and S5H), with baseline to re-feeding mean Z scores of 0.50 ± SEM 0.09 vs. −0.47 ± SEM 0.09, $p \leq 0.0001$ (Figure S5I). Similarly, but to a lesser extent, the mice also showed a rapid response to the delivery of caged, non-consumable food pellets. Now, 57.58% of the neurons were inhibited, 15.15% were activated, and 27.27% did not respond (Figures S5J and S5K), with baseline to re-feeding mean Z scores of 0.19 ± SEM 0.07 vs. −0.16 ± SEM 0.07, $p = 0.001$ (Figure S5L). Thus, PNOC/NPY neurons in the ARC show a clear, more-homogeneous suppression upon re-feeding compared with the global population of PNOC^{ARC} neurons.

Induced expression of *Npy* in PNOC-expressing cells increases food intake and body weight

After establishing the critical role of PNOC/NPY neurons in the regulation of feeding, we investigated whether the changes in *Npy* expression upon targeted disruption of the *Lepr* in PNOC neurons were attributable to either cluster #6 (PNOC+/NPY+/AgRP−) and/or cluster #7 (PNOC+/NPY+/AgRP+) neurons (Figures 6A–6D, S6A, and S6B). Assessing *Npy* mRNA expression, now in fasted and re-fed animals, clearly verified the overall increase of *Npy* expression in PNOC neurons of PNOC$^{\Delta LEPR}$ mice, consistent with the bacTRAP analysis performed in the random fed state. In addition, we found that the increase in *Npy* expression was only present in cluster #6 (PNOC+/NPY+/AgRP− neurons) (Figures 6A and 6B) but not in cluster #7

Figure 5. Activation of PNOC+/NPY+ cells in the ARC stimulates food intake

(A and B) (A) ARC delivery of an AAV vector expressing the stimulatory hM3D(Gq) DREADD receptor in a Cre-on/Flp-off (Con/Foff)-, Cre-off/Flp-on (Coff/Fon)-, or Cre-on-Flp-on (Con/Fon)-specific manner to PNOC-Cre, NPY-Flp, or PNOC-Cre::NPY-Flp mice creates (B) six experimental groups intersectionally targeting (1) no cells, (2) all NPY+ cells, (3) NPY+/PNOC− cells, (4) all PNOC+ cells, (5) PNOC+/NPY+ cells, or (6) PNOC+/NPY− cells.

(C–E) (C) Food intake 4 h following 1 mg/kg IP CNO treatment (morning, 8 a.m.) of each group. *In situ* hybridization was performed on brain slices from all groups 1 h after a CNO injection (1 mg/kg), followed by quantifications of (D) percent *Fos*+ PNOC cells and (E) percent *Fos*+ NPY cells.

(F and G) (F) Representative images showing the *Pnoc* (green), *Npy* (cyan), and *Fos* (magenta) mRNA expression in each group and (G) representative images depicting the expression of mCherry-immunolabeled neurons across these groups (red). Scale bars in (F) 50 μm and in (G) 100 μm. Data are represented as mean ± SEM, $n = 7$–11 (food intake) or $n = 3$–6 (*ISH*). p values calculated using one-way ANOVA followed by Tukey's multiple comparison test. *p ≤ 0.05; **p ≤ 0.01; ***p ≤ 0.001; ****p ≤ 0.0001.

See also Figure S5.

Please cite this article in press as: Solheim et al., Hypothalamic PNOC/NPY neurons constitute mediators of leptin-controlled energy homeostasis, Cell (2025), https://doi.org/10.1016/j.cell.2025.04.001

CellPress
OPEN ACCESS

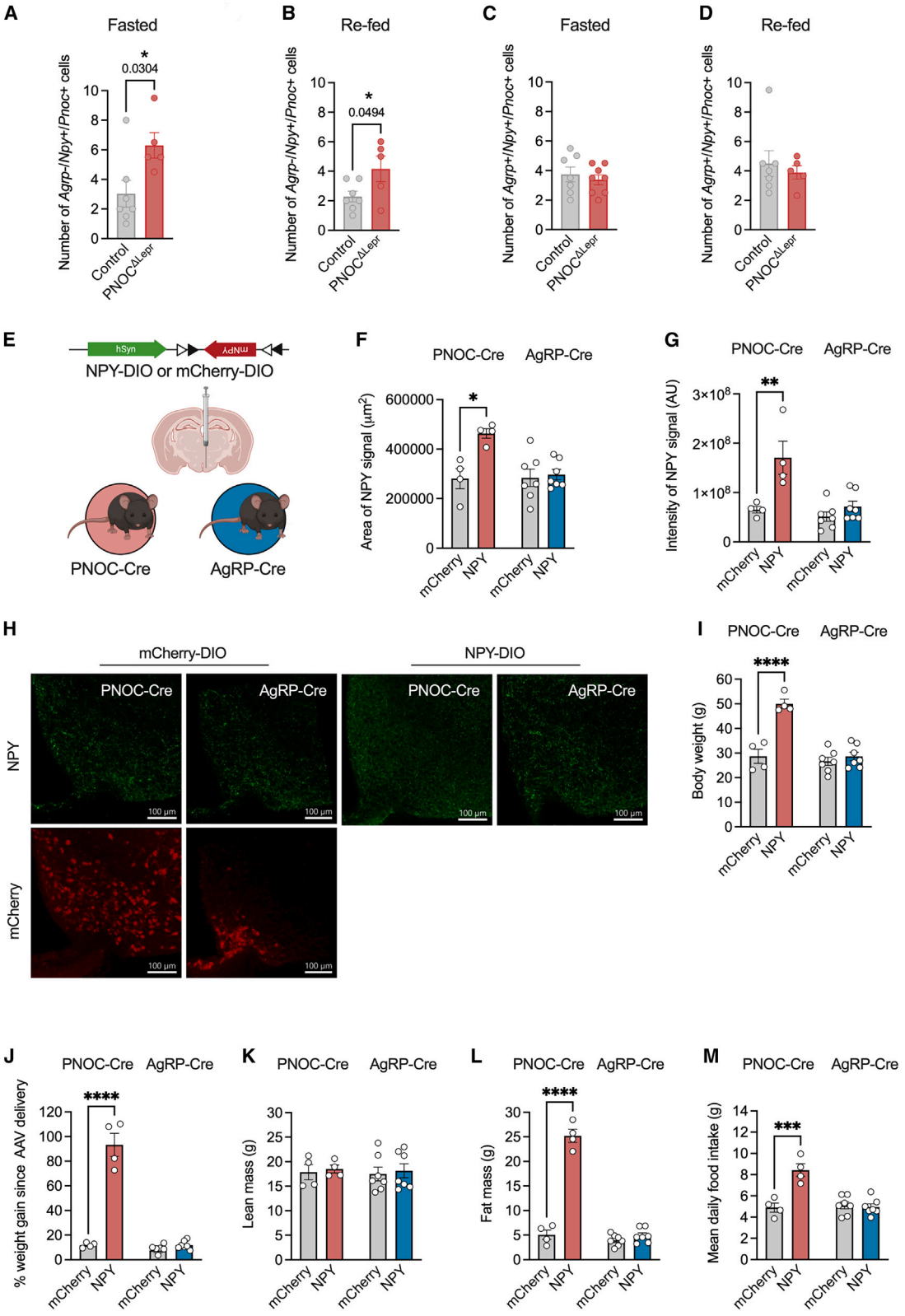

(legend on next page)

(PNOC+/NPY+/AgRP+ cells) (Figures 6C and 6D). Of note, comparative analysis of *Npy* expression in the clusters based on sn sequencing data revealed that cluster #7 cells in control mice exhibit a 7.86-fold higher expression level compared with cluster #6 (AgRP−) cells. The number of PNOC-/NPY+/AgRP+ cells were, importantly, not different between the genotypes (Figures S6C and S6D). Therefore, PNOC LEPR deficiency appears to predominantly upregulate *Npy* expression in cluster #6 cells, whereas baseline levels of *Npy* are lower compared with AgRP+ cluster #7 cells.

To further examine the functional role of enhanced *Npy* expression, we delivered an AAV allowing for Cre-dependent expression of *Npy* in the ARC of PNOC-Cre mice as well as AgRP-Cre mice (Figure 6E). NPY-AAV delivery in PNOC-Cre mice resulted in a significantly larger area of NPY immunoreactivity and higher signal intensity across the ARC compared with animals given a Cre-dependent mCherry-AAV (control) (Figures 6F–6H). Changes in NPY immunoreactivity signals between control animals and those given NPY-AAV were minimal in AgRP-Cre animals, possibly due to an already saturated expression of *Npy*. This is consistent with our previous results showing that employing this NPY-AAV to restore *Npy* expression in AgRP neurons of otherwise NPY-deficient mice restored *Npy* expression in AgRP neurons comparable with what is observed in control mice.[20,21] Remarkably, at time of sacrifice, PNOC-Cre mice given NPY-AAV weighed 21.4 g more than their control animals, whereas AgRP-Cre mice showed only a non-significant 2-gram difference (Figure 6I). In fact, already 4 weeks post AAV delivery, PNOC-Cre mice presented with a 90% higher weight gain (Figure 6J). uCT analysis showed that lean mass was unchanged, but the fat mass of PNOC-Cre mice given NPY-AAV increased 5-fold (Figures 6K and 6L). The weight gain was accompanied by a 1.7-fold increase in daily food intake (Figure 6M). Delivering the same AAV to AgRP-Cre animals had no effect on food intake or weight gain, further supporting the notion that the observed food regulatory role of PNOC/NPY cells is predominantly mediated via cluster #6 cells (Figures 6I–6M).

Cluster #6 PNOC+/NPY+/AgRP− neurons are conserved leptin-sensitive neurons in the human hypothalamus

Finally, we set out to validate the existence of the PNOC/NPY-expressing cells of cluster #6 in the human hypothalamus using our previously published reference atlas HYPOMAP, comprising sn sequencing and spatial transcriptomics.[22] Utilizing the cross-species cluster comparisons conducted in that study, we identified, for each murine PNOC^{ARC} cluster, its highest-correlated human cluster. This was possible for all clusters except for cluster #4 (Figures 7A and S7). We, however, observed substantial differences in gene expression conservation between conserved human and murine clusters: e.g., cluster #1 showed a markedly lower mean log-normalized expression of *PNOC* (0.14 in human vs. 1.08 in mouse) and also lacked expression of *HTR3B* in humans. We identified NPY+/AgRP+ neurons of cluster #7 in the human data, which very lowly expressed *PNOC* (0.03 mean log-normalized expression). Compellingly, we also identified a human population of *AGRP*-negative *NPY*-expressing cells corresponding to cluster #6, which exhibited the highest *PNOC* expression level (0.72 mean log-normalized expression) of all included clusters (Figures 7A and S7). Notably, we also detected *PNOC* expression in various other ARC clusters in human, highlighting again that gene expression is not fully conserved between humans and mice.

Next, we conducted *in situ* hybridization on tissue sections of human brain, which confirmed that the majority of human PNOC/NPY neurons do not express *AGRP* (*AGRP*− 70.37% ± SEM 10.40 and *AGRP*+ 29.63% ± SEM 10.40), supporting an important role of cluster #6 cells in humans as well as mice (Figures 7B and 7C). In a second *in situ* hybridization experiment, we were able to detect *LEPR* expression in human PNOC/NPY cells of the lateral ARC, thus confirming the conservation of *LEPR* in the cluster #6 cells (Figure 7D). Taken together, we demonstrate that, despite general differences in gene expression conservation of PNOC in human and murine ARC neurons, highly PNOC- and NPY-expressing cells of cluster #6 are present in both species, suggesting that these conserved neurons play an important role in the central regulation of energy homeostasis.

DISCUSSION

Recently, we showed that PNOC-expressing neurons of the ARC are activated upon acute HFD-feeding, leading to inhibition of anorexigenic POMC neurons and promoting hyperphagia.[13] Now, we demonstrate the critical role of PNOC LEPRs in regulating food intake under chow feeding conditions. We highlight their significant contribution to overall body weight control exerted by numerous neuronal cell types expressing *Leprs* and show that mice with *Lepr* re-expression exclusively in PNOC neurons have a considerably reduced body weight compared with global LEPR knockout (KO) mice. Consistently, both prenatal, whole-body PNOC *Lepr* ablation, as well as local

Figure 6. NPY overexpression in PNOC ARC neurons promotes hyperphagia and obesity

(A–D) (A) Number of AgRP−/PNOC+/NPY+ cells quantified from *in situ* hybridization analysis of control and PNOC$^{\Delta LEPR}$ animals in (A) 16 h fasted condition and (B) 1 h re-feeding following 16 h fast and the number of AgRP+/PNOC+/NPY+ cells in (C) fasted and (D) re-fed state. Data are represented as mean ± SEM. *p* values calculated using two-tailed unpaired Student's t test, $n = 5–7$ animals, 2 sections each.

(E) Schematic illustrating the experimental setup, where an mCherry-DIO control or NPY-DIO AAV was delivered bilaterally to the ARC of PNOC-Cre (red) or AgRP-Cre mice (blue).

(F and G) (F) Quantified area of NPY immunopositive signal after AAV injections and (G) intensity of signal.

(H) Representative images of immunopositive NPY signal in each group and the images depicting the spread and expression of Cre-dependent mCherry in both genotypes (red). Scale bars 100 μm.

(I–M) (I) Body weight 4 weeks after AAV delivery (J) percent weight gain, accompanied by (K) lean mass, (L) fat mass measured by uCT, and (M) daily food intake (3 weeks post AAV delivery). Data are represented as mean ± SEM, $n = 4–7$ mice of each genotype and treatment, *p* values calculated using one-way ANOVA followed by Tukey's multiple comparison test. *$p \leq 0.05$; **$p \leq 0.01$; ***$p \leq 0.001$; ****$p \leq 0.0001$.

See also Figure S6.

Please cite this article in press as: Solheim et al., Hypothalamic PNOC/NPY neurons constitute mediators of leptin-controlled energy homeostasis, Cell (2025), https://doi.org/10.1016/j.cell.2025.04.001

A

	PNOC^{ARC} Clusters	Human HYPOMAP clusters	Sn Avg exp PNOC	Sn % of all PNOC+
Crabp1	**Cluster 1 (Htr3b)** C185-103: Vgll3.Tbx3.GABA-1	C4-377 Mid-2 GABA-GLU-3 PDGFD ALDH1A1	0.14	5.01
Crabp1	**Cluster 2** (Tmem215) C185-104: Syt4.Tbx3.GABA-1	C4-376 Mid-2 GABA-GLU-3 PDGFD PGR	0.14	2.82
Satb2	**Cluster 3** (Nfix/Glp1r) C185-127: Nfix.Satb2.GABA-6	C4-62 Mid-1 GABA-1 SHISAL2B	0.47	15.95
Otp	**Cluster 4 (Chst9/Nts)** C185-119: Nts.Sst.GABA-4	N/A	N/A	N/A
Otp	**Cluster 5 (Sst/Unc13c)** C185-118: Otp.Sst.GABA-4	C4-359 Mid-2 GABA-GLU-1 RGS22 NDNF	0.01	0.21
Otp	**Cluster 6 (Sst/Npy)** C185-117: Npy.Sst.GABA-4	C4-357 Mid-2 GABA-GLU-1 RGS22 NPY	0.72	8.45
Otp	**Cluster 7** (Agrp/Npy) C66-46: Agrp.GABA-4	C4-355 Mid-2 GABA-GLU-1 RGS22 AGRP	0.03	1.36
	Other ARC	Other ARC	0.14	66.22

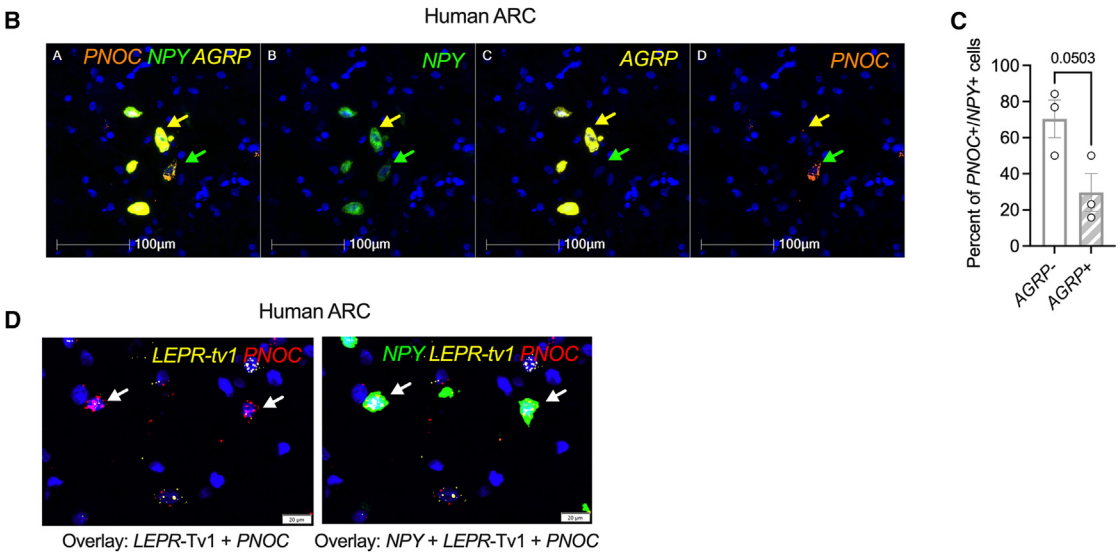

Figure 7. PNOC/NPY/LEPR neurons are conserved in the human hypothalamus

(A) Table with overview of seven PNOC ARC clusters shown in Figures 3A and 3B and their best-correlated human clusters. Genes used to mark clusters in *in situ* hybridization (ISH) validation are marked as bold and underlined. Columns from left to right: (1) murine cluster name and identifier; (2) corresponding human HYPOMAP cluster identifier; (3) sn avg exp PNOC: average PNOC expression in in ARC clusters of human HYPOMAP; and (4) sn% of all PNOC+: percent of all PNOC-expressing cells in ARC clusters of human HYPOMAP.

(B and C) (B) Representative images of *PNOC* (orange), *NPY* (green), and *AgRP* (yellow) mRNA expression in human ARC, with left image displaying all 3 channels and right images displaying each channel separately. Yellow arrow highlights a PNOC+/NPY+/AGRP+ cell and green arrow highlights PNOC+/NPY+/AGRP− cells. Scale bars 100 µm.(C) Quantitative analysis showing percent of PNOC+/NPY+ cells with or without *AgRP* expression.

(D) Representative image of mRNA expression in human lateral ARC, same image displayed twice, left image indicating overlap of *PNOC* (red), *LEPR* (yellow), and right image overlaying with *NPY* (green). Scale bars 20 µm. Data in (C) are represented as mean ± SEM, $n = 3$. Representative images (B and D) from $n = 3$. p values calculated using two-tailed unpaired Student's t test.

See also Figure S7.

PNOC^{ARC}-restricted ablation in adult mice, cause hyperphagia. Furthermore, we identify a distinct group of PNOC-expressing cells in the ARC co-expressing *Lepr* and *Npy* that account for the observed hyperphagia within the otherwise molecularly heterogeneous cell population.

Recent insight into the diverse nature of POMC neurons has forced a re-evaluation of the leptin-melanocortin model.[8] Although POMC neurons likely are direct targets of leptin for the control of glucose metabolism, leptin appears to play a minor role in activating POMC neurons to suppress feeding in adult mice.[9,16,23,24] The mild body weight variations that were observed in earlier POMC LEPR KO studies may result from the consequences of *Lepr* deletion or re-expression from immature future non-POMC neurons, including those that later become NPY neurons.[25,26]

Please cite this article in press as: Solheim et al., Hypothalamic PNOC/NPY neurons constitute mediators of leptin-controlled energy homeostasis, Cell (2025), https://doi.org/10.1016/j.cell.2025.04.001

In contrast, selective ablation of LEPRs in GABAergic neurons of mice results in largely increased food intake and body weight, similar to that of global LEPR KO, highlighting their dominant role in leptin's effect on energy balance.[27] Although developmental KO of LEPRs in AgRP neurons showed only minor effects on body weight,[10] CRISPR-Cas9-mediated inactivation of *Lepr* in AgRP neurons of adolescent or adult mice resulted in a pronounced obese phenotype, although to varying degrees in different studies.[11,12] Leptin action in AgRP neurons alone, however, does not explain the full effect of leptin, consequently arguing for the involvement of other GABAergic neurons.[10–12] More recently, a study identified previously unrecognized GABAergic populations of hypothalamic LEPR neurons, including *LeprTbx19*, *LeprFoxb1*, *LeprOpn5*, and *LeprGlp1r* cells.[28] The authors continue to show that the GABAergic neurons in the DMH co-expressing *Lepr* and glucagon-like peptide-1 receptor (*Glp1r)* control food intake, with little effect on glucose metabolism. Interestingly, re-expression of *Lepr* in GLP1R-positive neurons on a *Lepr*-deficient background significantly attenuates the body weight gain observed upon body-wide LEPR deficiency.[28] Although a small portion of PNOC-expressing cells is also located in the DMH, we do not observe PNOC^{DMH} leptin-induced pSTAT3 signaling, disclosing PNOC^{ARC} neurons as a distinct population from these. Similarly, a recent study revealed a population of GABAergic thyrotropin-releasing hormone (*Trh*)-expressing neurons in the ARC that express *Glp1r* and that, upon Glp1-stimulation, inhibit AgRP neurons.[29] A recently described GABAergic neuronal population in the ARC, characterized by the expression of basonuclin 2 (*Bnc2)*, inhibits AgRP neurons through leptin-mediated activation and becomes rapidly activated upon sensory food perception and re-feeding *in vivo*.[30] Interestingly, this cell population exhibits molecular similarities to the TRH/GLP1R neurons as well as LEPR/GLP1R-positive neurons identified by Rupp et al.,[28] except that BNC2 neurons are dispensable for the food-intake-lowering effect of long-acting GLP1 agonists.[30] Although all of these neuronal populations are activated by leptin or feeding, PNOC/NPY neurons identified here are robustly and homogenously inhibited upon re-feeding.

Although PNOC neurons are widely distributed across the brain, we have identified and validated seven distinct PNOC populations residing within the ARC. Through bacTRAP profiling, we reveal that PNOC^{ARC} cells upregulate *Npy* expression in PNOC$^{\Delta LEPR}$ mice (Figure 4). Two out of seven PNOC clusters are characterized by *Npy* expression (cluster #6: PNOC+/NPY+/AgRP− neurons, and cluster #7: PNOC+/NPY+/AgRP+ cells). Chemogenetic activation of PNOC+/NPY+ cells (i.e., clusters #6 and #7) potently promotes feeding to the same extent as chemogenetic activation of all PNOC^{ARC} neurons, whereas chemogenetic activation of the majority of PNOC neurons, the *Npy*-negative clusters #1–5, fails to modulate food intake (Figure 5). Of note, the intersectional targeting approach predominantly activated *Agrp*− cluster #6 PNOC+/NPY+ cells compared with cluster #7 AgRP+ cells (84.3% for cluster #6 vs. 15.7% for cluster #7) (Figure S5). This demonstrates that PNOC+/NPY+ cells (predominantly cluster #6, i.e., AgRP- cells) exert the stimulatory food intake effect of global PNOC^{ARC} neuron activation.

In addition, we find that, upon PNOC LEPR KO, *Npy* expression is upregulated in cluster #6 (PNOC+/NPY+/AgRP− neurons) but not in cluster #7 (PNOC+/NPY+/AgRP+ neurons) (Figure 6). Furthermore, Cre-dependent AAV-mediated overexpression of *Npy* in PNOC^{ARC} neurons leads to hyperphagia and massive obesity, whereas *Npy* expression using the same AAV in AgRP neurons has no effect on food intake and body weight. Together, this demonstrates that leptin action in cluster #6 (PNOC+/NPY+/AgRP− neurons) regulates body weight via *Npy* expression. This is further supported by our observation that this cluster exhibits the highest proportion of *Lepr* expression (78%) compared with all other PNOC^{ARC} clusters, coinciding with previous data showing that *Lepr* expression is higher in the subset of NPY neurons that do not express *Agrp*.[31] In line with our study, *Agrp*-negative NPY^{ARC} neurons were also recently found to drive feeding under positive energy balance, with leptin acting directly on them.[32,33] The authors describe an orexigenic population of non-AgRP cells that, upon DREADD stimulation in *ad libitum* HFD-feeding conditions, causes increased food intake along with increased translation of NPY.[33] Similar to PNOC-expressing neurons, these also show a stronger response to HFD than to chow condition.[13] Although AgRP neurons can inhibit food intake by suppressing POMC neurons via GABA release,[34] studies have shown that the inhibition of POMC neurons in HFD-fed obese mice occurs independent of AgRP neurons.[35] In contrast, HFD feeding rapidly activates PNOC^{ARC} neurons and inhibits POMC neurons via GABAergic input, highlighting an important difference in their regulation in obesity.[13] In fact, chemogenetic inhibition of PNOC^{ARC} neurons abrogates the diet-induced inhibition of POMC neurons.[19] Therefore, PNOC^{ARC} cluster #6 cells likely represent the cell type responsible for this diet-induced inhibition. This notion is further supported by our *in vivo* single-cell Ca^{2+} imaging of PNOC/NPY neurons, where they are almost homogenously inhibited upon re-feeding, thereby likely representing the previously identified 20% inhibited subclass of the global PNOC^{ARC} population sensitive to obesity-induced disinhibition.

Excitingly, we find that PNOC^{ARC} cell clusters are largely conserved in the human hypothalamus, with the exception of the murine PNOC^{ARC} cluster #4, characterized by the expression of *Otp*, *Nts*, and *Chst9*.[22] Despite large similarities in gene expression between the murine and human PNOC^{ARC} clusters, there are also substantial differences: cluster #1 in mice is characterized by co-expression of *Crabp1* and *Htr3b*, but we cannot detect *HTR3B* expression in the human hypothalamus. However, the functionally relevant cell type identified in the present study, i.e., cluster #6 murine PNOC+/NPY+/AgRP− neurons, are highly conserved in humans and represent a 3-times-more-prevalent population in humans than the orthologs of murine cluster #7 cells (PNOC+/NPY+/AgRP+).

In summary, our experiments identify PNOC neurons as a hypothalamic cell population regulated by leptin to control energy homeostasis and that PNOC LEPRs are vital for body weight maintenance. We further discover that this regulation occurs through a highly specialized, molecularly defined subset of PNOC/LEPR/NPY neurons also found in humans, which holds

great promise for the development of future targeted obesity therapeutics.

Limitations of the study

Recent work has revealed the necessity to investigate hypothalamic neurons in control of metabolism at higher granularity than previously considered.[9] This is also highlighted by the high degree of heterogeneity of PNOC^{ARC} neurons identified here. We have firmly narrowed the food-intake-regulatory function of the global PNOC^{ARC} population to a specific subpopulation (10% of all PNOC^{ARC} neurons) as PNOC/NPY cells. Furthermore, we provide complementary lines of evidence that a subpopulation of those, i.e., cluster #6 cells (PNOC+/NPY+/AgRP− neurons), but not PNOC+/NPY+/AgRP+ neurons (cluster #7), likely represents the most relevant food-intake-regulatory PNOC^{ARC} subpopulation. This is based on their selective upregulation of *Npy* expression upon LEPR deletion, the clear obesity-inducing effect of *Npy* expression in PNOC neurons and their predominant targeting in the intersectional chemogenetic approach. Nevertheless, given the limitations of currently available intersectional targeting tools, we have not succeeded in exclusively activating this AgRP-negative cell type. This certainly will be subject to future studies, along with identifying selective or enriched genes in this specific PNOC^{ARC} cluster to make them amendable to pharmacological intervention.

RESOURCE AVAILABILITY

Lead contact

Further information and requests for resources and reagents should be directed to the lead contact, Jens C. Brüning (bruening@sf.mpg.de).

Materials availability

HTR3B-Cre mice generated for the study are available from the lead contact with a completed materials transfer agreement. AAV-gLepr are available from Garron T. Dodd.

Data and code availability

Raw and fully processed RNA-seq data from bacTRAP-based ribosomal profiling of PNOC neurons are deposited in the NCBI Gene Expression Omnibus under accession code GEO: GSE292416. All data and code are available upon reasonable request.

ACKNOWLEDGMENTS

We are grateful to the donors and their families for the generous tissue donations and to Professor Colin Smith at The Edinburgh Brain and Tissue Bank for providing human brain tissue samples. We thank members of the lab for helpful discussions; Jens Alber, Andreas Beyrau, Christian Heilinger, Pia Scholl, Christiane Schäfer (all from MPI-MR), and Jeanette Bannebjerg Johansen (Novo Nordisk A/S) for excellent technical assistance; and Ramona Braun, Christine Hausen, Anna Sieben, and Ursula Lichtenberg for their administrative guidance. All schematic diagrams in the manuscript were created with BioRender.com. This work was funded in part by Novo Nordisk (to J.C.B.), the Center for Molecular Medicine Cologne (CMMC) (to J.C.B.), the German National Diabetes Center (DZD) (to J.C.B.), the European Research Council (ERC) grant (SYNEME: 742106 to J.C.B.), the National Health and Medical Research Council (to G.T.D., 2022/GNT2021126 and 2020/GNT2002427), the Australian Research Council (to G.T.D., DP220102910), Diabetes Australia (to G.T.D., Y23G-DODG), and the University of Melbourne Dean's Innovation Award (to G.T.D.).

AUTHOR CONTRIBUTIONS

M.H.S. and J.C.B. conceived the study, wrote the manuscript, and oversaw all aspects of the research. M.H.S., S.S., W.C., P.S.S., C.A.B., D.W-L., A.d.R.-M. F.T.W., and T.S.-H. performed experiments and interpreted data. P.K. and L.S. performed computational analysis and interpreted data. C.A.B. and G.T.D. provided unique CRISPR-Cas9 resources. A.S. and S.L. provided human samples, designed and performed experiments, and interpreted data. All co-authors reviewed and agreed on the final version of the manuscript.

DECLARATION OF INTERESTS

J.C.B. is a co-founder of Cerapeutix and has received research funding through collaborations with Sanofi Aventis and Novo Nordisk Inc., and he also consulted for Eli Lilly and Company and Novo Nordisk, all of which did not affect the content of this article. S.L. and A.S. are Novo Nordisk employees and minor shareholders as part of an employee offering program. G.T.D. is a founder of Gallant Bio and has received research funding from Eli Lilly and Company and Novo Nordisk, all of which did not affect the content of this article.

STAR★METHODS

Detailed methods are provided in the online version of this paper and include the following:

- KEY RESOURCES TABLE
- EXPERIMENTAL MODEL AND SUBJECT DETAILS
  - Animal care
  - Animal diets
  - Mouse lines
  - Generation of experimental mouse lines
- METHOD DETAILS
  - Analysis of body composition
  - Indirect calorimetry and food intake
  - Insulin tolerance tests (ITTs)
  - Glucose tolerance tests (GTTs)
  - Organ harvest and histological analysis
  - Plasma collection and analysis by enzyme-linked immunosorbent assays (ELISAs)
  - Stereotactic surgical procedures and viral deliveries
  - PCR validation of Crispr-Cas9 *Lepr* genome editing
  - Miniscope single neuron imaging experiments
  - Data analysis of inscopix single neuron imaging
  - Chemogenetic activation of neurons
  - BacTRAP-based ribosomal profiling
  - RNA sequencing
  - Analysis of bacTRAP RNA-sequencing data
  - Analysis of single-cell RNA-sequencing data
  - Leptin-stimulated pSTAT3 and immunohistochemistry
  - AAV-based NPY expression and immunohistochemistry
  - RNA *in situ* hybridization
  - Imaging and quantifications
  - Statistics

Received: March 27, 2024
Revised: December 23, 2024
Accepted: April 1, 2025
Published: April 23, 2025

REFERENCES

1. Boutari, C., and Mantzoros, C.S. (2022). A 2022 update on the epidemiology of obesity and a call to action: as its twin COVID-19 pandemic appears to be receding, the obesity and dysmetabolism pandemic continues to rage on. Metabolism *133*, 155217. https://doi.org/10.1016/j.metabol.2022.155217.

2. Zhang, Y., Proenca, R., Maffei, M., Barone, M., Leopold, L., and Friedman, J.M. (1994). Positional cloning of the mouse obese gene and its human homologue. Nature *372*, 425–432. https://doi.org/10.1038/372425a0.

3. Farooqi, I.S., and O'rahilly, S. (2005). Monogenic obesity in humans. Annu. Rev. Med. *56*, 443–458. https://doi.org/10.1146/annurev.med.56.062904.144924.

4. Friedman, J.M., and Halaas, J.L. (1998). Leptin and the regulation of body weight in mammals. Nature *395*, 763–770. https://doi.org/10.1038/27376.

5. Elmquist, J.K., Ahima, R.S., Maratos-Flier, E., Flier, J.S., and Saper, C.B. (1997). Leptin activates neurons in ventrobasal hypothalamus and brainstem. Endocrinology *138*, 839–842. https://doi.org/10.1210/endo.138.2.5033.

6. Elias, C.F., Kelly, J.F., Lee, C.E., Ahima, R.S., Drucker, D.J., Saper, C.B., and Elmquist, J.K. (2000). Chemical characterization of leptin-activated neurons in the rat brain. J. Comp. Neurol. *423*, 261–281.

7. Brüning, J.C., and Fenselau, H. (2023). Integrative neurocircuits that control metabolism and food intake. Science *381*, eabl7398. https://doi.org/10.1126/science.abl7398.

8. Lavoie, O., Michael, N.J., and Caron, A. (2023). A critical update on the leptin-melanocortin system. J. Neurochem. *165*, 467–486. https://doi.org/10.1111/jnc.15765.

9. Biglari, N., Gaziano, I., Schumacher, J., Radermacher, J., Paeger, L., Klemm, P., Chen, W., Corneliussen, S., Wunderlich, C.M., Sue, M., et al. (2021). Functionally distinct POMC-expressing neuron subpopulations in hypothalamus revealed by intersectional targeting. Nat. Neurosci. *24*, 913–929. https://doi.org/10.1038/s41593-021-00854-0.

10. van de Wall, E., Leshan, R., Xu, A.W., Balthasar, N., Coppari, R., Liu, S.M., Jo, Y.H., MacKenzie, R.G., Allison, D.B., Dun, N.J., et al. (2008). Collective and individual functions of leptin receptor modulated neurons controlling metabolism and ingestion. Endocrinology *149*, 1773–1785. https://doi.org/10.1210/en.2007-1132.

11. Xu, J., Bartolome, C.L., Low, C.S., Yi, X., Chien, C.H., Wang, P., and Kong, D. (2018). Genetic identification of leptin neural circuits in energy and glucose homeostases. Nature *556*, 505–509. https://doi.org/10.1038/s41586-018-0049-7.

12. Zhu, C., Jiang, Z., Xu, Y., Cai, Z.L., Jiang, Q., Xu, Y., Xue, M., Arenkiel, B.R., Wu, Q., Shu, G., et al. (2020). Profound and redundant functions of arcuate neurons in obesity development. Nat. Metab. *2*, 763–774. https://doi.org/10.1038/s42255-020-0229-2.

13. Jais, A., Paeger, L., Sotelo-Hitschfeld, T., Bremser, S., Prinzensteiner, M., Klemm, P., Mykytiuk, V., Widdershooven, P.J.M., Vesting, A.J., Grzelka, K., et al. (2020). PNOC^{ARC} Neurons Promote Hyperphagia and Obesity upon High-Fat-Diet Feeding. Neuron *106*, 1009–1025.e10. https://doi.org/10.1016/j.neuron.2020.03.022.

14. Steuernagel, L., Lam, B.Y.H., Klemm, P., Dowsett, G.K.C., Bauder, C.A., Tadross, J.A., Hitschfeld, T.S., Del Rio Martin, A., Chen, W., de Solis, A.J., et al. (2022). HypoMap-a unified single-cell gene expression atlas of the murine hypothalamus. Nat. Metab. *4*, 1402–1419. https://doi.org/10.1038/s42255-022-00657-y.

15. Hardaway, J.A., Halladay, L.R., Mazzone, C.M., Pati, D., Bloodgood, D.W., Kim, M., Jensen, J., DiBerto, J.F., Boyt, K.M., Shiddapur, A., et al. (2019). Central Amygdala Prepronociceptin-Expressing Neurons Mediate Palatable Food Consumption and Reward. Neuron *102*, 1037–1052.e7. https://doi.org/10.1016/j.neuron.2019.03.037.

16. Berglund, E.D., Vianna, C.R., Donato, J., Jr., Kim, M.H., Chuang, J.C., Lee, C.E., Lauzon, D.A., Lin, P., Brule, L.J., Scott, M.M., et al. (2012). Direct leptin action on POMC neurons regulates glucose homeostasis and hepatic insulin sensitivity in mice. J. Clin. Invest. *122*, 1000–1009. https://doi.org/10.1172/JCI59816.

17. Platt, R.J., Chen, S., Zhou, Y., Yim, M.J., Swiech, L., Kempton, H.R., Dahlman, J.E., Parnas, O., Eisenhaure, T.M., Jovanovic, M., et al. (2014). CRISPR-Cas9 knockin mice for genome editing and cancer modeling. Cell *159*, 440–455. https://doi.org/10.1016/j.cell.2014.09.014.

18. Hernandez, J., Fabelo, C., Perez, L., Moore, C., Chang, R., and Wagner, E.J. (2019). Nociceptin/orphanin FQ modulates energy homeostasis through inhibition of neurotransmission at VMN SF-1/ARC POMC synapses in a sex- and diet-dependent manner. Biol. Sex Differ. *10*, 9. https://doi.org/10.1186/s13293-019-0220-3.

19. Sotelo-Hitschfeld, T., Minère, M., Klemm, P., Borgmann, D., Wnuk-Lipinski, D., Jais, A., Jia, X., Corneliussen, S., Kloppenburg, P., Fenselau, H., et al. (2024). GABAergic disinhibition from the BNST to PNOC^{ARC} neurons promotes HFD-induced hyperphagia. Cell Rep. *43*, 114343. https://doi.org/10.1016/j.celrep.2024.114343.

20. Engström Ruud, L., Pereira, M.M.A., de Solis, A.J., Fenselau, H., and Brüning, J.C. (2020). NPY mediates the rapid feeding and glucose metabolism regulatory functions of AgRP neurons. Nat. Commun. *11*, 442. https://doi.org/10.1038/s41467-020-14291-3.

21. Chen, W., Mehlkop, O., Scharn, A., Nolte, H., Klemm, P., Henschke, S., Steuernagel, L., Sotelo-Hitschfeld, T., Kaya, E., Wunderlich, C.M., et al. (2023). Nutrient-sensing AgRP neurons relay control of liver autophagy during energy deprivation. Cell Metab. *35*, 786–806.e13. https://doi.org/10.1016/j.cmet.2023.03.019.

22. Tadross, J.A., Steuernagel, L., Dowsett, G.K.C., Kentistou, K.A., Lundh, S., Porniece, M., Klemm, P., Rainbow, K., Hvid, H., Kania, K., et al. (2025). A comprehensive spatio-cellular map of the human hypothalamus. Nature *639*, 708–716. https://doi.org/10.1038/s41586-024-08504-8.

23. Balthasar, N., Coppari, R., McMinn, J., Liu, S.M., Lee, C.E., Tang, V., Kenny, C.D., McGovern, R.A., Chua, S.C., Jr., Elmquist, J.K., et al. (2004). Leptin receptor signaling in POMC neurons is required for normal body weight homeostasis. Neuron *42*, 983–991. https://doi.org/10.1016/j.neuron.2004.06.004.

24. Üner, A.G., Keçik, O., Quaresma, P.G.F., De Araujo, T.M., Lee, H., Li, W., Kim, H.J., Chung, M., Bjørbæk, C., and Kim, Y.B. (2019). Role of POMC and AgRP neuronal activities on glycaemia in mice. Sci. Rep. *9*, 13068. https://doi.org/10.1038/s41598-019-49295-7.

25. Padilla, S.L., Carmody, J.S., and Zeltser, L.M. (2010). Pomc-expressing progenitors give rise to antagonistic neuronal populations in hypothalamic feeding circuits. Nat. Med. *16*, 403–405. https://doi.org/10.1038/nm.2126.

26. Yu, H., Rubinstein, M., and Low, M.J. (2022). Developmental single-cell transcriptomics of hypothalamic POMC neurons reveal the genetic trajectories of multiple neuropeptidergic phenotypes. eLife *11*, e72883. https://doi.org/10.7554/eLife.72883.

27. Vong, L., Ye, C., Yang, Z., Choi, B., Chua, S., Jr., and Lowell, B.B. (2011). Leptin action on GABAergic neurons prevents obesity and reduces inhibitory tone to POMC neurons. Neuron *71*, 142–154. https://doi.org/10.1016/j.neuron.2011.05.028.

28. Rupp, A.C., Tomlinson, A.J., Affinati, A.H., Yacawych, W.T., Duensing, A.M., True, C., Lindsley, S.R., Kirigiti, M.A., MacKenzie, A., Polex-Wolf, J., et al. (2023). Suppression of food intake by Glp1r/Lepr-coexpressing neurons prevents obesity in mouse models. J. Clin. Invest. *133*, e157515. https://doi.org/10.1172/JCI157515.

29. Webster, A.N., Becker, J.J., Li, C., Schwalbe, D.C., Kerspern, D., Karolczak, E.O., Bundon, C.B., Onoharigho, R.A., Crook, M., Jalil, M., et al. (2024). Molecular connectomics reveals a glucagon-like peptide 1-sensitive neural circuit for satiety. Nat. Metab. *6*, 2354–2373. https://doi.org/10.1038/s42255-024-01168-8.

30. Tan, H.L., Yin, L., Tan, Y., Ivanov, J., Plucinska, K., Ilanges, A., Herb, B.R., Wang, P., Kosse, C., Cohen, P., et al. (2024). Leptin-activated hypothalamic BNC2 neurons acutely suppress food intake. Nature *636*, 198–205. https://doi.org/10.1038/s41586-024-08108-2.

31. Lee, N.J., Qi, Y., Enriquez, R.F., Clarke, I., Ip, C.K., Wee, N., Baldock, P.A., and Herzog, H. (2020). Energy partitioning between fat and bone mass is controlled via a hypothalamic leptin/NPY relay. Int. J. Obes. (Lond.) *44*, 2149–2164. https://doi.org/10.1038/s41366-020-0550-6.

32. Lee, N.J., Oraha, J., Qi, Y., Enriquez, R.F., Tasan, R., and Herzog, H. (2023). Altered function of arcuate leptin receptor expressing

neuropeptide Y neurons depending on energy balance. Mol. Metab. *76*, 101790. https://doi.org/10.1016/j.molmet.2023.101790.

33. Qi, Y., Lee, N.J., Ip, C.K., Enriquez, R., Tasan, R., Zhang, L., and Herzog, H. (2023). Agrp-negative arcuate NPY neurons drive feeding under positive energy balance via altering leptin responsiveness in POMC neurons. Cell Metab. *35*, 979–995.e7. https://doi.org/10.1016/j.cmet.2023.04.020.
34. Cowley, M.A., Smart, J.L., Rubinstein, M., Cerdán, M.G., Diano, S., Horvath, T.L., Cone, R.D., and Low, M.J. (2001). Leptin activates anorexigenic POMC neurons through a neural network in the arcuate nucleus. Nature *411*, 480–484. https://doi.org/10.1038/35078085.
35. Rau, A.R., and Hentges, S.T. (2017). The Relevance of AgRP Neuron-Derived GABA Inputs to POMC Neurons Differs for Spontaneous and Evoked Release. J. Neurosci. *37*, 7362–7372. https://doi.org/10.1523/JNEUROSCI.0647-17.2017.
36. Chen, Y., Essner, R.A., Kosar, S., Miller, O.H., Lin, Y.C., Mesgarzadeh, S., and Knight, Z.A. (2019). Sustained NPY signaling enables AgRP neurons to drive feeding. eLife *8*, e46348. https://doi.org/10.7554/eLife.46348.
37. Tong, Q., Ye, C.P., Jones, J.E., Elmquist, J.K., and Lowell, B.B. (2008). Synaptic release of GABA by AgRP neurons is required for normal regulation of energy balance. Nat. Neurosci. *11*, 998–1000. https://doi.org/10.1038/nn.2167.
38. Schindelin, J., Arganda-Carreras, I., Frise, E., Kaynig, V., Longair, M., Pietzsch, T., Preibisch, S., Rueden, C., Saalfeld, S., Schmid, B., et al. (2012). Fiji: an open-source platform for biological-image analysis. Nat. Methods *9*, 676–682. https://doi.org/10.1038/nmeth.2019.
39. Giovannucci, A., Friedrich, J., Gunn, P., Kalfon, J., Brown, B.L., Koay, S.A., Taxidis, J., Najafi, F., Gauthier, J.L., Zhou, P., et al. (2019). CaImAn an open source tool for scalable calcium imaging data analysis. eLife *8*, e38173. https://doi.org/10.7554/eLife.38173.
40. Patel, H., Ewels, P., Peltzer, A., Botvinnik, O., Sturm, G., Moreno, D., Vemuri, P., Garcia, M.U., silviamorins., Pantano, L., et al. (2023). nf-core/rnaseq: nf-core/rnaseq v3.12.0 - Osmium Octopus (3.12.0). Zenodo. https://doi.org/10.5281/zenodo.7998767.
41. Patro, R., Duggal, G., Love, M.I., Irizarry, R.A., and Kingsford, C. (2017). Salmon provides fast and bias-aware quantification of transcript expression. Nat. Methods *14*, 417–419. https://doi.org/10.1038/nmeth.4197.
42. Love, M.I., Huber, W., and Anders, S. (2014). Moderated estimation of fold change and dispersion for RNA-seq data with DESeq2. Genome Biol. *15*, 550. https://doi.org/10.1186/s13059-014-0550-8.
43. Cohen, P., Zhao, C., Cai, X., Montez, J.M., Rohani, S.C., Feinstein, P., Mombaerts, P., and Friedman, J.M. (2001). Selective deletion of leptin receptor in neurons leads to obesity. J. Clin. Invest. *108*, 1113–1121. https://doi.org/10.1172/JCI13914.
44. Daigle, T.L., Madisen, L., Hage, T.A., Valley, M.T., Knoblich, U., Larsen, R.S., Takeno, M.M., Huang, L., Gu, H., Larsen, R., et al. (2018). A Suite of Transgenic Driver and Reporter Mouse Lines with Enhanced Brain-Cell-Type Targeting and Functionality. Cell *174*, 465–480.e22. https://doi.org/10.1016/j.cell.2018.06.035.
45. Heiman, M., Schaefer, A., Gong, S., Peterson, J.D., Day, M., Ramsey, K.E., Suárez-Fariñas, M., Schwarz, C., Stephan, D.A., Surmeier, D.J., et al. (2008). A translational profiling approach for the molecular characterization of CNS cell types. Cell *135*, 738–748. https://doi.org/10.1016/j.cell.2008.10.028.
46. Zhang, M., Pan, X., Jung, W., Halpern, A.R., Eichhorn, S.W., Lei, Z., Cohen, L., Smith, K.A., Tasic, B., Yao, Z., et al. (2023). Molecularly defined and spatially resolved cell atlas of the whole mouse brain. Nature *624*, 343–354. https://doi.org/10.1038/s41586-023-06808-9.

Please cite this article in press as: Solheim et al., Hypothalamic PNOC/NPY neurons constitute mediators of leptin-controlled energy homeostasis, Cell (2025), https://doi.org/10.1016/j.cell.2025.04.001

STAR★METHODS

KEY RESOURCES TABLE

REAGENT or RESOURCE	SOURCE	IDENTIFIER
Antibodies		
Phospho-Stat3 (Tyr705), Polyclonal Rabbit	Cell Signaling Technology	Cat# 9131; RRID: AB_331586
Anti-GFP, Polyclonal Chicken	Abcam	Cat# 13970; RRID: AB_300798
Polyclonal secondary, Goat	Thermo Fisher Scientific	Cat# A-11012; RRID: AB_2534079
Fluorescein (FITC) AffiniPure™ Goat Anti-Chicken IgY (IgG) (H+L)	Jackson ImmunoResearch Inc.	Cat# 103-095-155; RRID: AB_2337384
NPY, Monoclonal, Rabbit	Cell Signaling Technology	Cat# 11976; RRID: AB_2716286
mCherry, Monoclonal Antibody (16D7)	Invitrogen	Cat# M11217; RRID: AB_2536611
Alexa Fluor 647, Donkey Polyclonal anti-Rabbit IgG (H+L)	Invitrogen	Cat# A-31573; RRID: AB_2536183
Alexa 594, Donkey Polyclonal anti-Rat igG (H+L)	Invitrogen	Cat# A-21209; RRID: AB_2535795
GFP, monoclonal	Memorial Sloan-Kettering Monoclonal Antibody Facility	Cat# Htz-GFP-19F7; RRID: AB_2716736
GFP, monoclonal	Memorial Sloan-Kettering Monoclonal Antibody Facility	Cat# Htz-GFP-19C8; RRID: AB_2716737
Bacterial and virus strains		
AAV-gLepR	This paper	N/A
AAV9-nEF-Con/Fon-DREADD-Gq-mCherry	Addgene plasmid, packaged by VectorBiolabs	Cat# 183532; RRID: Addgene_183532
AAV9-nEF-Con/Foff-DREADD-Gq-mCherry	Addgene plasmid, packaged by VectorBiolabs	Cat# 183533; RRID: Addgene_183533
AAV9-nEF-Coff/Fon-DREADD-Gq-mCherry	Addgene plasmid, packaged by VectorBiolabs	Cat# 183534; RRID: Addgene_183534
AAV8-EF1a-Con/Fon-GCamp6m	Addgene	Cat# 137119-AAV8; RRID: Addgene_137119
AAV9-hSyn-DIO-mCherry	Addgene	Cat# 50459-AAV9; RRID: Addgene_50459
AAV8-EF1a-DIO-mNPY-WPRE-1	Assoc. Prof. Zachary A. Knight	Chen et al.[36]
Chemicals, peptides, and recombinant proteins		
Murine Leptin, recombinant	Preprotech/Thermo Fisher	Cat# 450-31
Glucose, 20% solution	B. Braun Melsungen AG	PZN 04164483
Saline, NaCl 0.9% solution	B. Braun Melsungen AG	PZN 01957160
Human Insulin	Lilly Pharma	
Buprenorphine	Bayer	PZN 01498870
Meloxicam	Boehringer Ingelheim	PZN 07578423
Isofluorane	Dräger and Piramal Healthcare	N/A
Clozapine-*N*-Oxide (CNO)	Abcam	Cat# 141704
Dimethyl sulfoxide (DMSO)	Sigma Aldrich	Cat# 276855
Sucrose	Sigma Aldrich	Cat# 57-50-1
Paraformaldehyde	Sigma Aldrich	Cat# 30525-89-4
UltraPure Phenol:Chloroform:Isoamyl Alcohol	Invitrogen/Thermo Fisher Scientific	Cat# 15593031
Critical commercial assays		
RNAscope Fluorescent Multiplex Detection Reagents v2	ACD	Cat# 323100
RNAscope LS multiplex fluorescent reagent kit	ACD	Cat# 322800
RNAscope LS 4-Plex Ancillary Kit Multiplex Reagent Kit	ACD	Cat# 322830
Basescope Detection Reagents v2 RED	ACD	Cat# 323910

(*Continued on next page*)

Please cite this article in press as: Solheim et al., Hypothalamic PNOC/NPY neurons constitute mediators of leptin-controlled energy homeostasis, Cell (2025), https://doi.org/10.1016/j.cell.2025.04.001

Continued

REAGENT or RESOURCE	SOURCE	IDENTIFIER
RNAscope Wash Buffer	ACD	Cat# 310091
RNAscope Target Retrieval Reagent	ACD	Cat# 322000
RNAscope Protease Plus	ACD	Cat# 322331
RNAscope Protease III	ACD	Cat# 222337
RNAscope probe Mm-Egfp	ACD	Cat# 492011
RNAscope probe Mm-cFos	ACD	Cat# 316921
RNAscope probe Mm-AgRP	ACD	Cat# 400711
RNAscope probe Mm-Npy	ACD	Cat# 313321
RNAscope probe Mm-Pnoc	ACD	Cat# 437881
RNAscope probe Mm-Lepr-Tv1	ACD	Cat# 471171
RNAscope probe Mm-Htr3b	ACD	Cat# 497541
RNAscope probe Mm-Crabp1	ACD	Cat# 474711
RNAscope probe Mm-Satb2	ACD	Cat# 413261
RNAscope probe Mm-Chst9	ACD	Cat# 522181
RNAscope probe Mm-Sst	ACD	Cat# 437881
RNAscope probe Hs-Agrp	ACD	Cat# 557458
RNAscope probe Hs-Npy	ACD	Cat# 416678
RNAscope probe Hs-Pnoc	ACD	Cat# 1045248
RNAscope probe Hs-Lepr-tv1	ACD	Cat# 410378
Basescope probe Mm-Lepr	ACD	Cat# 895341
Basescope probe Mm-Pnoc	ACD	Cat# 1199261
Opal 520 Fluorophore	Akoya Bioscience	Cat# FP1487001KT
Opal 570 Fluorophore	Akoya Bioscience	Cat# FP1488001KT
Opal 650 Fluorophore	Akoya Bioscience	Cat# FP1496001KT
Opal 690 Fluorophore	Akoya Bioscience	Cat# FP1497001KT
iFluor488	AAT Bioquest/VWR	Cat# 45020
iFluor546	AAT Bioquest/VWR	Cat# 45025
iFlour594	AAT Bioquest/VWR	Cat# 45035
Ultra-Sensitive Mouse Insulin ELISA Kit	Crystal Chem	Cat# 90080
Mouse Leptin ELISA Kit	Crystal Chem	Cat# 90030
Protein A Dynabeads	Invitrogen	Cat# 10334693
Complete mini EDTA-free protease inhibitor	Roche	Cat# 411836153001
PhosSTOP	Roche	Cat# 11921681001
RNAeasy Micro kit	Qiagen	Cat# 74104
RNA 6000 Nano Kit	Agilent Technologies	Cat# 5067-1511
RNA 6000 Nano Ladder	Agilent Technologies	Cat# 5067-1529
Illumina Nextera XT DNA sample preparation kit	Illumina	N/A
Peqlab KAPA Library Quantification Kit	Roche	N/A
Applied Biosystems 7900HT Sequence Detection	Applied Bioysystems	N/A
Deposited data		
RNAseq	This paper	NCBI GEO: GSE292416
Experimental models: Organisms/strains		
C57BL/6N	Charles River	Strain #027
PNOC-EGFP	Jackson Laboratories	Stock #038517
PNOC-Cre	Jais et al.[13]	N/A
LEPR-Flox	Jackson Laboratories	Stock #008327

(*Continued on next page*)

Please cite this article in press as: Solheim et al., Hypothalamic PNOC/NPY neurons constitute mediators of leptin-controlled energy homeostasis, Cell (2025), https://doi.org/10.1016/j.cell.2025.04.001

Continued

REAGENT or RESOURCE	SOURCE	IDENTIFIER
$LEPR^{LOXTB}$	Jackson Laboratories	Stock #018989
Rosa26-Cas9-EGFP	Jackson Laboratories	Stock #024858
L10a-GFP	Biglari. et al.[9]	N/A
HTR3B-Cre	This paper	N/A
NPY-Flp	Jackson Laboratories	Stock #030211
AgRP-Cre	Tong et al.[37]	Stock #012899
Software and algorithms		
GraphPad Prism (Version 10)	GraphPad Software Inc.	https://www.graphpad.com/scientific-software/prism/
Fiji/ImageJ software/Adiposoft plugin	Schindelin et al.[38]	https://imagej.net/software/fiji/
SoftMax Pro 6.3 software	Molecular devices	https://www.moleculardevices.com/products/microplate-readers/acquisition-and-analysis-software/softmax-pro-software
Imaris version (Version 9.9)	Bitplane AG	https://imaris.oxinst.com/versions/9-9
HALO software	Indica Labs	https://indicalab.com/halo/
R Studio	The R Foundation for Statistical Computing, Institute for Statistics and Mathematics, University of Economics and Business, Austria	https://www.r-project.org
Biorender	Biorender	https://biorender.com
Inscopix Data Acquisition Software (Version 1.6.0)	Inscopix	https://iq.inscopix.com/software
CNMF-E	Giovannucci et al.[39]	N/A
IVIS Living Image Software V4.3.1, and Vinci software package 4.61.0.	Caliper Life Science, Perkin Elmer	http://www.perkinelmer.de/category/in-vivo-imaging-software
CRISPR MIT	Massachusetts Institute of Technology, USA	http://crispr.mit.edu
CRISPR ChopChop	University of Bergen, Norway	http://chopchop.cbu.uib.no
CRISPR Off spotter	Thomas Jefferson University, USA	https://cm.jefferson.edu/Off-Spotter
nfcore rnaseq Analysis pipeline version 3.12.0	Patel et al.[40]	https://nf-co.re/about
Salmon 1.10.1	Patro et al.[41]	N/A
DESeq2 package, version 1.38.3	Love et al.[42]	N/A
Seurat (v5.0.1), ggplot2 (v3.4.4), schex (v1.16.1) and ggtree (v3.10.0) R packages	R Studios	N/A
Other		
Normal Chow Diet	ssniff Spezialdiäten GmbH	Cat# V1554
Contour Blood Glucose Meter	Bayer	N/A
Contour Next strips	Bayer	Cat# #84167879
Metabond Quick Adhesive Cement System	Parkell	SKU: S380
GRIN lens 7.3mm length, NA 0.5	Inscopix	N/A
ImmEdge hydrophobic barrier pen	Vector Laboratories	Cat# 310018
SuperFrost Ultra Plus™ GOLD Adhesion Slides	Thermo Fisher Scientific	Cat# 11976299
Vectashield Antifade Mounting-Medium with DAPI	Vector Laboratories	Cat# H-1200
Leica TCS SP-8-X Confocal microscope	Leica Microsystems	https://www.leica-microsystems.com/products/confocal-microscopes/
Leica Stellaris 8 Confocal microscope	Leica Microsystems	https://www.leica-microsystems.com/products/confocal-microscopes/

(*Continued on next page*)

Please cite this article in press as: Solheim et al., Hypothalamic PNOC/NPY neurons constitute mediators of leptin-controlled energy homeostasis, Cell (2025), https://doi.org/10.1016/j.cell.2025.04.001

Continued

REAGENT or RESOURCE	SOURCE	IDENTIFIER
Olympus VS200 slide scanner	Olympus	https://www.olympus-lifescience.com/
Zeiss Meta 710 Confocal Laser Scanning Microscope	Zeiss	https://www.zeiss.com/microscopy/int/products/confocal-microscopes.html
Leica BOND RX Fully Automated Research Stainer (Human ISH)	Leica Biosystems	https://www.leicabiosystems.com/us/ihc-ish/ihc-ish-instruments/bond-rx/
IVIS Spectrum CT *In Vivo* Imaging System	Caliper LifeScience, Perkin Elmer	https://resources.perkinelmer.com/lab-solutions/resources/docs/bro_010459b_01%20prd_spectrumct.pdf
Stereotaxic frame	David Kopf Instruments	https://inscopix.com
nVista System	Inscopix	N/A
2100 Bioanalyzer Instrument	Agilent Technologies	Part Number:G2939BA
Phenomaster	TSE Systems	https://www.tse-systems.com/service/phenomaster/
FilterMax F5 Multi-Mode microplate reader	Molecular devices	https://www.moleculardevices.com/products/microplate-readers/multi-mode-readers/filtermax-f3-f5-readers
Stainless-steel brain matrix	World precision instruments	https://www.wpiinc.com
Homogenizer	Potter S, Braun	N/A
Ovation RNASeq System (V2)	Tecan	N/A
Agilent 2200 TapeStation	Agilent	N/A
Illumina HiSeq 4000 sequencing instrument	Illumina	N/A
Invitrogen Qubit System	Invitrogen	N/A

EXPERIMENTAL MODEL AND SUBJECT DETAILS

Animal care

All animal experiments were in compliance with protocols approved by local government authorities (Bezirksregierung Köln). The permission to maintain and breed mice was issued by the Department for Environment and Consumer Protection - Veterinary Section, Köln, North Rhine-Westphalia, Germany. Animals were kept on a C57Bl/6N background and housed in groups up to five animals per cage. Mice were kept on a 12-hour light/dark cycle in individually ventilated cages (IVCs) at 22°C–24°C. When male cohorts are indicated, a full female cohort has been analyzed in parallel and showed comparable results. Otherwise, experimental groups are a mix of male and female animals.

Animal diets

Animals had *ad libitum* access to water and food. All mice were fed a chow-diet (Ssniff V1554, 59494 Soest, Germany) containing 57% of calories from carbohydrates, 34% calories from protein and 9% calories from fat. Food was only withdrawn during defined fasting periods (overnight, 16 h).

Mouse lines

C57BL/6N: Mice were obtained from Charles River, France.

PNOC-EGFP (BAC-transgenic): Mice are available at the Jackson Laboratories, USA (Stock #038517). To maintain the line in our facility at the Max Planck Institute for Metabolism Research, Cologne, Germany mice were bred with C57BL/6N mice from Charles River, France. The mouse line has previously been described.[13]

PNOC-Cre: Mice were bred with C57BL/6N mice from Charles River, France, to maintain the line in our facility. Their generation has been previously described.[13]

LEPR-Flox: Mice were obtained from the Jackson Laboratories, USA (Stock #008327) and have been previously described.[43] Mice were maintained by intercross (homozygous) in our facilities at the Max Planck Institute for Metabolism Research, Cologne, Germany.

$LEPR^{LoxTB}$: Mice were obtained from the Jackson Laboratories (Stock #018989) and have been described previously.[16] Mice were bred with C57BL/6N mice from Charles River, France, to maintain the line heterozygous (homozygous mice are infertile).

Rosa26-Cas9-EGFP: Previously described mice[17] were obtained from the Jackson Laboratories (Stock #024858). Mice were maintained by intercross (homozygous) in our facilites.

L10a-GFP: Cre-dependent ROSA26-STOP-L10a-GFP Fl/Fl, mice were obtained by intercross (homozygous) at the Max Planck Institute for Metabolism Research, Cologne, Germany. Their generation has been previously described by our laboratory[9]

HTR3B-Cre: These mice (Htr3bP2ACre) were generated by Crispr-Cas9 techniques. Two gRNAs around the stop codon of *Htr3b* (Htr3b5guide: CCGAATCTACCTTGCCGTGC, Htr3b3guide: TGTGGAGCAGAATGTGACAA) were co-injected with Cas9 protein and a repair template that introduces a P2A-driven Cre in frame to *Htr3b* into C57BL/6 oocytes:

AACTCTCTTCGAACTCGGGATCAGATTCACCAGAAGGAGGTGGAGTGGCTGGCCATCCTGTATCGCTTTGATCAGCTGCTCTTC
CGAATCTACCTTGCCGTGCTtGGGCTCTATACCGTCACCTTATGCTCTCTCTGGGCACTGTGGAGCAGAATGGGGCGCGCCGGCA
GCGGCGCCACCAACTTCAGCCTGCTGAAGCAGGCCGGCGACGTGGAGGAGAACCCCGGCCCCgccaccATGCCCAAGAAGAAG
AGGAAGGTGTCCAATTTACTGACCGTACACCAAAATTTGCCTGCATTACCGGTCGATGCAACGAGTGATGAGGTTCGCAAGAACC
TGATGGACATGTTCAGGGATCGCCAGGCGTTTTCTGAGCATACCTGGAAAATGCTTCTGTCCGTTTGCCGGTCGTGGGCGGCATG
GTGCAAGTTGAATAACCGGAAATGGTTTCCCGCAGAACCTGAAGATGTTCGCGATTATCTTCTATATCTTCAGGCGCGCGGTCTGG
CAGTAAAAACTATCCAGCAACATTTGGGCCAGCTAAACATGCTTCATCGTCGGTCCGGGCTGCCACGACCAAGTGACAGCAATGC
TGTTTCACTGGTTATGCGGCGGATCCGAAAAGAAAACGTTGATGCCGGTGAACGTGCAAAACAGGCTCTAGCGTTCGAACGCACT
GATTTCGACCAGGTTCGTTCACTCATGGAAAATAGCGATCGCTGCCAGGATATACGTAATCTGGCATTTCTGGGGATTGCTTATAA
CACCCTGTTACGTATAGCCGAAATTGCCAGGATCAGGGTTAAAGATATCTCACGTACTGACGGTGGGAGAATGTTAATCCATATTG
GCAGAACGAAAACGCTGGTTAGCACCGCAGGTGTAGAGAAGGCACTTAGCCTGGGGGTAACTAAACTGGTCGAGCGATGGATTT
CCGTCTCTGGTGTAGCTGATGATCCGAATAACTACCTGTTTTGCCGGGTCAGAAAAAATGGTGTTGCCGCGCCATCTGCCACCAG
CCAGCTATCAACTCGCGCCCTGGAAGGGATTTTTGAAGCAACTCATCGATTGATTTACGGCGCTAAGGATGACTCTGGTCAGAGA
TACCTGGCCTGGTCTGGACACAGTGCCCGTGTCGGAGCCGCGCGAGATATGGCCCGCGCTGGAGTTTCAATACCGGAGATCAT
GCAAGCTGGTGGCTGGACCAATGTAAATATTGTCATGAACTATATCCGTAACCTGGATAGTGAAACAGGGGCAATGGTGCGCCTG
CTGGAAGATGGCGATTAgAGACCGCTGGTCTCACTTGATATGGGGTTACAACATGTAGGGAAAGCTGAACAGTGCTTGGAGAGGG
TCTGAAAAGAAGGGGTGGGTAGCCTCCAGGATGCTATTGT

Offspring was genotyped using 5Htr3btyp: GTCCCCGGTCCATCAGGAGCAT, 3Htr3btyp: GTCAATAGCCAATAAGATACTT, 3Cre: ATGTTTAGCTGGCCCAAATGTTG primers to obtain a targeted 623 bp, or 393 bp WT band, in standard PCR conditions.

NPY-Flp: Npy-IRES2-FlpO-D mice were obtained from the Jackson Laboratories (Stock #030211) and have been described previously.[44] Mice were bred with C57BL/6N mice from Charles River, France, to maintain the line heterozygous.

Agrp-Cre: Mice were obtained from breeding in house in our facilities. Their generation has been described previously.[37]

Generation of experimental mouse lines

PNOC$^{\Delta LEPR}$

Heterozygous transgenic PNOC-Cre mice were crossed with homozygous LEPR-Flox mice, and further bred to generate homozygosity for the LEPR-flox allele to generate PNOC-Cre Tg/WT::LEPR Fl/Fl mice. Cre-negative LEPR-Flox littermates were used as controls.

PNOC-Cre$^{\Delta PNOC}$/PNOC-Cre$^{\Delta LEPR\,\Delta PNOC}$

PNOC-Cre mice express Cre-recombinase while simultaneously disrupting the PNOC coding Exon 2. PNOC-Cre$^{\Delta PNOC}$ mice were created by breeding PNOC-Cre mice to homozygosity (PNOC Tg/Tg), heterozygous PNOC-Cre mice were used in paired experiments as their controls. Similarly, PNOC-Cre$^{\Delta LEPR\Delta PNOC}$ mice were created by breeding PNOC$^{\Delta LEPR}$ with each other (PNOC-Cre Tg/Tg::Lepr Fl/Fl). Littermates with heterozygous Cre-expression were used as controls for the same experiments.

PNOC-Cre::LEPR^{LoxTB}

Heterozygous PNOC-Cre mice were crossed with heterozygous LEPR^{LoxTB} mice. PNOC-Cre Tg/WT::LEPR^{LoxTB} Fl/WT mice were further bred with LEPR^{LoxTB} Fl/WT mice to generate homozygosity, creating the 3 experimental groups: LEPR^{LoxTB} (PNOC-Cre WT/WT::LEPR^{LoxTB} Fl/Fl), PNOC-Cre::LEPR^{LoxTB} (PNOC-Cre Tg/WT::LEPR^{LoxTB} Fl/Fl), and controls as either PNOC-Cre WT/WT::LEPR^{LoxTB} WT/WT or PNOC-Cre WT/WT::LEPR^{LoxTB} Fl/WT.

PNOC-Cre^{Cas9}

Heterozygous PNOC-Cre mice were crossed with homozygous Rosa26-Cas9-EGFP creating PNOC-Cre Tg/WT::Cas9 Fl/WT mice or controls mice (either PNOC-Cre WT/WT:: Cas9 Fl/WT or PNOC-Cre Tg/WT).

PNOC-Cre$^{\Delta LEPR\text{-}L10a\text{-}EGFP}$

Knockout group were generated by breeding PNOC-Cre$^{\Delta LEPR}$ mice with LEPR Fl/Fl::L10a-GFP Fl/Fl animals creating PNOC-Cre Tg/WT::LEPR-Flox Fl/Fl::L10a-GFP Fl/WT animals. Control mice were generated from a separate but parallel breeding of PNOC-Cre directly with L10a-GFP-flox mice producing PNOC-Cre Tg/WT::LEPR-Flox WT/WT::L10a-GFP Fl/WT.

HTR3B$^{\Delta LEPR}$

Heterozygous transgenic HTR3B-Cre mice were crossed with homozygous LEPR-Flox mice, and further bred to generate homozygosity for the LEPR-flox allele to generate HTR3B-Cre Tg/WT::LEPR Fl/Fl mice. Cre-negative LEPR-Flox littermates were used as controls.

HTR3B-Cre$^{L10a\text{-}EGFP}$

Mice were generated by breeding HTR3B-Cre with L10a-GFP-flox mice producing HTR3B-Cre Tg/WT::L10a-GFP Fl/WT.

Please cite this article in press as: Solheim et al., Hypothalamic PNOC/NPY neurons constitute mediators of leptin-controlled energy homeostasis, Cell (2025), https://doi.org/10.1016/j.cell.2025.04.001

PNOC-Cre::Npy-Flp

Heterozygous Pnoc-Cre mice were bred with heterozygous NPY-Flp animals creating mice for all study groups: Pnoc-Cre Tg/WT::NPY-Flp WT/WT, Pnoc-Cre WT/WT::NPY-Flp Frt/WT, Pnoc-Cre Tg/WT::NPY-Flp Frt/WT, and Pnoc-Cre WT/WT::NPY-Flp WT/WT.

METHOD DETAILS

Analysis of body composition

Body weights were assessed weekly. Lean and fat mass was analyzed by micro-computed tomography (micro-CT)-based imaging of isoflurane-anesthetized mice (Dräger and Piramal Healthcare) at 15-17 weeks of age. Data acquisition was performed in an IVIS Spectrum CT-scanner (Calpier LifeScience, USA) using the IVIS LivingImage Software V4.3.1. Quantification of fat mass was determined with a modification of the Vinci software package 4.61.0.

Indirect calorimetry and food intake

Metabolic measurements were obtained using the PhenoMaster (TSE systems), an open circuit calorimetry system. Mice were acclimatized for at least 3 days prior to analysis. Food and water was provided ad libitum in the appropriate devices. For fasting and refeeding experiments, bedding was changed and food hoppers were removed overnight for 16 h before reinstated. Ambient temperature was consistent at 22°C, and measurements were taken automatically every 20 min.

Insulin tolerance tests (ITTs)

ITTs were performed in random fed mice at 11-12 weeks of age. Basal blood glucose concentrations were measured before receiving an intraperitoneal injection (IP) of 0.75 U/kg bodyweight of human insulin (Lilly Pharma) and continued measuring blood glucose concentrations again at 15-, 30- and 60-min post injection. Blood glucose concentrations were measured from whole venous blood using an automatic glucose monitor (Contour, Bayer HealthCare, Germany) averaging value from two monitors per animal. Prior to the test mice were placed in fresh cages and food was withdrawn over the whole course of the experiment.

Glucose tolerance tests (GTTs)

GTTs were performed in mice that had been fasted overnight (16h) at 12-13 weeks of age. Basal blood glucose concentrations were measured before receiving an intraperitoneal injection (IP) of 20% glucose (10 mL/kg bodyweight, B.Braun) and continued measuring blood glucose concentrations again at 15-, 30-, 60- and 120-min post injection. Blood glucose concentrations were measured from whole venous blood using an automatic glucose monitor (Contour, Bayer HealthCare, Germany) averaging value from two monitors per animal. Food was withdrawn over the whole course of the experiment.

Organ harvest and histological analysis

Fat tissues were dissected out, weighted and then a piece of tissue was fixed for 48 h in 4% formalin. Tissues were paraffin embedded, sectioned and stained with hematoxylin and eosin. Adipocyte area was determined using the Fiji software (Adiposoft plugin).

Plasma collection and analysis by enzyme-linked immunosorbent assays (ELISAs)

Whole blood from mice was collected into EDTA containing tubes from tail. Samples where then centrifuged at 5,000xg for 30 min at 4°C. The liquid component (plasma) was collected and stored at -80°C until use. Plasma insulin was measured in duplicates according to the instructions by the manufacturer, using the Ultra sensitive Mouse Insulin ELISA Kit (Crystal Chem, Cat #90080) and Mouse Leptin ELISA Kit (Crystal Chem, #90030). Readout using optical density was determined using a FilterMax F5 Multi-Mode microplate reader and SoftMax Pro 6.3 software (Molecular Devices). Readings at 630 nm were subtracted from readings at 450 nm to correct for optical imperfections, and quantification were done using a four-parameter curve-fit standard curve. HOMA-IR was defined as fasting glucose (mmol/L) x fasting insulin (μmol/L)/22.5).

Stereotactic surgical procedures and viral deliveries

Mice were anesthetized by isoflurane and positioned onto a stereotaxic frame (David Kopf Instruments). To relieve post-operative pain mice received buprenorphine (0.1 mg/kg) and meloxicam (5 mg/kg). For three days after the procedure mice received meloxicam in their drinking water. Adeno-associated virus (AAV) was injected at 100 nL per minute into the ARC (AP: -1.5 mm; ML: ± 0.3 mm; DV: -5.85 mm) and the glass pipette was withdrawn 5 min after injection. 200 nl AAV was bilaterally injected, with the exception of miniscope experiments.

To generate the AAV-gLepR (pAAV[-U6>mLepr[gRNA- GGTAAACTTCCCTCGAGGTC]-U6>mLepr[gRNA-TCTGACGTACCTACG GAGTC]-CAG>LL:rev(mCherry):rev(LL):WPRE) viral vector, sgRNAs were designed using online CRISPR tools (http://crispr.mit.edu and http://chopchop.cbu.uib.no/) with minimal off-target gRNA binding predicted by Off-Spotter (https://cm.jefferson.edu/Off-Spotter/). For the AAV-gLepR a pUp-U6>mLepr[gRNA-GGTAAACTTCCCTCGAGGTC]-U6>mLepr[gRNA- TCTGACGTACCTACG GAGTC] gRNA vector was generated using the Gibson assembly of a AarI digested pUp-U6-gRNA-AarI-Stuffer-AarI backbone. The p-Up vectors were cloned alongside pDown-CAG and pTail-LL:rev(mCherry):rev(LL) to generate the final vector by LR reaction

using the Gateway method. The AAV plasmid were used to generate recombinant viral vectors packaged into the AAV-DJ/8 pseudotype. For chemogenetic experiments AAV9-nEF-Con/Fon-DREADD-Gq- Cherry (Addgene 183532), AAV9-nEF-Con/Foff-DREADD-Gq- Cherry (Addgene 183533) and AAV9-nEF-Coff/Fon-DREADD-Gq- Cherry (Addgene 183534) was used (a gift from Karl Deisseroth & the INTRSECT 2.0 Project). AAV8-EF1a-DIO-NPY virus (kindly provided by Dr. Z. Knight[36]) or control virus AAV8-hSyn-DIO-mCherry was delivered for NPY overexpression.

PCR validation of Crispr-Cas9 *Lepr* genome editing

To confirm targeted genome editing in hypothalamus biopsies from hypothalamus, amygdala and tail was collected from control and KO animals. Genomic DNA was isolated using phenol-chloroform extraction. Lysed samples were added an equal volume of phenol-chloroform containing Isoamyl alcohol (1:1:24). After centrifugation at high speed the upper aqueous phase containing DNA was transferred to a fresh tube containing 1 ml isopropanol. Sample was centrifuged to get a pellet, and supernatant was discarded. Pellets were washed 2x in 70% ethanol and airdried before being resuspended in TE buffer containing RNAse. *Lepr* has multiple splice forms. From the ENSMUST00000037552.10 Lepr-201 transcript we targeted coding exon 7-9 (exon 8-10, if considering one untranslated exon). GuideRNA 1 lies in coding exon 7 of *Lepr* long isoform, gRNA 2 in exon 9. PCR primers were designed to cover 3.48 kb genomic DNA, that upon crispr-cas9 editing gives a 307 bp band. Leprdeletionfw: TCTGACTAGTGTTGGATCGAATGC. Leprdeletionrev: ACAGCCAATCATCTTCTCAATTACTCTA.

Miniscope single neuron imaging experiments

500 nl of AAV8-EF1a-Con/Fon-GCamp6m (addgene 137119) was injected into the ARC using the coordinates AP -1.45; ML -0,2; DV -5,85 at a titer of 2.4x1013. pAAV-EF1a-Con/Fon-GCaMP6M was a gift from Karl Deisseroth & INTRSECT 2.0 Project (Addgene viral prep # 137119-AAV8). Three weeks post AAV delivery, a straight cuffed GRIN (gradient index) lens with integrated baseplate (0.5 NA, 1/2 pitch, 0.6 x 7.3 mm, Inscopix Palo Alto, CA, USA) was surgically implanted intracranially under isoflurane anesthesia. After skin removal, the scull was treated with a dental etching gel for roughening the cranial calotte (Super-Bond-C&B kit, Sun Medical Co., LTD, Japan) to improve dental cement adhesion. The GRIN lens was then placed above the ARC following the coordinates AP-0.48; ML -0.3, with the stereotaxic arm positioned at a -8° angle. The DV coordinates were adjusted based on each animal's increase in GCAMP6s fluorescence during implant insertion with final positioning between 5.60 and 5.70. The lens was fixed to the scull using MetaBond adhesive cement (Parkwell S380). To visualize GCaMP6 expression, light-emitted diode (LED)-driven excitation (1.2 mW/mm^2) was used with a wavelength of 475/10 nm. The emitted light (approx. 475/50nm, green) was detected by epifluorescence miniscope (Inscopix Palo Alto, CA, USA).

Before initiating experiments, mice were trained for 5 consecutive days with a dummy camera. Mice were kept in their home cage throughout the recordings. For both refeeding and caged food experiments mice were fasted overnight 16h. Recordings contained 15-minute measurement of baseline neuronal activity followed by 15-minutes to capture changes in PNOC/NPY neuronal activity in response to refeeding/ caged food. Recordings were acquired with 10 frames per second (fps), with a gain intensity between 6 to 7 and LED power between 15-20%.

Data analysis of inscopix single neuron imaging

Videos were preprocessed, registered and motion corrected with IDPS (Inscopix Data Processing Software) and saved as .tiff files. Single cell data was extracted with CaImAn (Calcium Imaging Analysis), a Python toolbox and open-source library for large-scale calcium imaging data analysis.[39] With CaImAn, the Constrained Nonnegative Matrix Factorization for micro-Endoscopic data (CNMF-E) algorithm was used on .tiff neuronal videos for automatic neuron identification. After manual check-up, neurons and their corresponding traces were extracted from the output, where each trace represented the activity of a neuron over a specific time period. Per experiment, neuronal traces were exported as .csv files for subsequent clustering analysis, *Z* score calculation and visualization.

For each neuron, a *Z* score was computed based on the mean and standard deviation of its baseline activity period (pre-intervention). This *Z* score transformation standardized each neuron's activity relative to its own baseline. Next, the *Z* scored traces of neurons underwent a clustering process. Cosine dissimilarity was used as the distance metric to measure the angular difference between *Z* scored traces. The k-medoids clustering algorithm was further applied with a predetermined value of k = 3, resulting in the classification of neurons into three distinct clusters based on their response to the intervention: Up: Neurons with increased signal compared to baseline, non-responder: neurons with unchanged signal relative to baseline; down: neurons with reduced signal compared to baseline.

Chemogenetic activation of neurons

Mice were housed individually and acclimatized in experimental cages (TSE system) for optimal habituation to food hoppers and water dispensers before the experiment. Clozapine-N-Oxide (CNO) was dissolved in Dimethyl sulfoxide (DMSO) to a concentration of 10 mg/ml and further diluted in Saline. For food intake measurements in the TSE system, all mice received IP injections of Saline or CNO (1 mg/kg body weight) in the early light phase (morning 8 am) on separate days. 1 h before deep anesthesia, transcardial perfusion and brain harvest, animals were again injected with CNO, in the absence of food, to activate the neurons.

BacTRAP-based ribosomal profiling

Affinity purification of translating ribosomes was carried out as described by Heiman et al.[45] with minor adaptions. Immediately after sacrifice, hypothalamic samples from random fed mice (10–12-week-old) dissected out using a stainless-steel brain matrix (World precision instruments) and directly snap frozen in liquid nitrogen. Protein A Dynabeads (375 μl per IP, Invitrogen) were washed 3x in 0.15M KCl IP wash buffer (20 mM HEPES [pH 7.4], 5 mM $MgCl_2$, 150 mM KCl, 1% NP40, 0.5 mM DTT and 100 μg/ml cycloheximide). Beads were subsequently resuspended in 275 μl 0.15M KCl IP wash buffer and loaded with 50 μg of 19C8 and 50 μg of 19F7 (Cat# Htz-GFP-19F7 and Htz-GFP-19C8, Memorial Sloan Kettering Monoclonal Antibody Facility) and rotated over night at 4°C. Pooled hypothalamic tissue (4 pooled animals per sample; 4 samples per group) was homogenized in lysis buffer (20 mM HEPES [pH 7.4], 5 mM $MgCl_2$, 150 mM KCl, 0.5 mM DTT, 40 U/ml RNasin, 100 μg/ml cycloheximide, protease and phosphatase inhibitor cocktails [1 tablet of cOmplete mini EDTA-free protease inhibitor cocktail/7 mL and 2 tablets of PhosSTOP/10 ml]) 2x at 250 rpm, and 9x at 750 rpm on a rotating glass/teflon potter homogenizer (Potter S, Braun) at 4°C. Homogenates were transferred to microcentrifuge tubes (Nonstick, RNase-free microfuge tubes, 1.5 ml, Ambion, Invitrogen) and centrifuged at 2,000xg for 10 min at 4°C. Working on ice, the supernatant was transferred to a new tube, and 1/9 sample volume 10% NP-40 (final concentration: 1%) and 1/9 sample volume 300 mM DHPC (final concentration: 30 mM) was added. Solution was then incubated on ice for 2 min and before centrifuging at 17,000xg, 10 min at 4°C. The supernatant was moved to a new tube, and a 25 μl aliquot was removed, transferred to a new tube, flash frozen in liquid nitrogen and stored at 80°C for purification as input RNA. For immunoprecipitation (IP) 200 μl of antibody-bound magnetic beads were added to the remaining supernatant (800-1000 μl supernatant) and incubated at 4°C, 1h rotating. The magnetic beads were collected and resuspended in 1000 μl of 0.35 M KCl IP wash buffer (20 mM HEPES [pH 7.4], 5 mM $MgCl_2$, 350 mM KCl, 1% NP40, 0.5 mM DTT, 100 μg/ml cycloheximide). Beads were washed 3x more in 1000 μl of 0.35 M KCl IP wash buffer, and then collected. The RNA was eluted by addition of buffer RLT (350 μL) to the beads, allowed to incubate at RT for 5 minutes and RNA was purified subsequently using the RNeasy Micro Kit (QIAGEN). RNA integrity was assessed using an Agilent 2100 bioanalyzer.

RNA sequencing

Whole transcriptome amplification was performed using the Ovation RNASeq System (V2)(Tecan, Mannedorf, Switzerland). Total RNA was used for first strand cDNA synthesis, with both poly(T) and random primers, followed by second strand synthesis and isothermal strand-displacement amplification. Sequencing libraries were generated using the Illumina Nextera XT DNA sample preparation kit (San Diego, CA, USA), with 1 ng cDNA input. After validation (Agilent 2200 TapeStation) and quantification (Invitrogen Qubit System) all transcriptome libraries were pooled. The pool was quantified using the Peqlab KAPA Library Quantification Kit and the Applied Biosystems 7900HT Sequence Detection and sequenced on an Illumina HiSeq 4000 sequencing instrument with a 2x75bp paired-end read length.

Analysis of bacTRAP RNA-sequencing data

The RNA sequencing data analysis was conducted using the community-curated community-curated nfcore rnaseq analysis pipeline version 3.12.0 (Patel et al. 2023[40]). Gene-level quantification was performed using Salmon 1.10.1,[41] with the GRCm38 reference genome serving as the basis for alignment. For the differential gene expression analysis, the DESeq2 package, version 1.38.3,[42] implemented in R, was employed. A gene was considered to be enriched in PNOC neurons if it exhibited differential expression under one of two conditions: (1) Control-IP vs Control-Input or (2) $PNOC^{\Delta LEPR}$-IP vs $PNOC^{\Delta LEPR}$-Input ($p_{adj} \leq 0.05$ and $log\ 2\ fc \geq 0.5$). Differentially expressed genes due to LEPR KO were identified by comparing $PNOC^{\Delta LEPR}$-IP vs Control-IP ($p_{adj} \leq 0.05$) and filtered for enrichment in PNOC-expressing neurons.

Analysis of single-cell RNA-sequencing data

We used our previously published reference atlas HypoMap to define PNOC populations and extract marker genes and annotations.[14] Potential ARC clusters on cluster level C185 were defined using the existing region prediction, followed by manual curation using publicly available spatial transcriptomics data to remove likely misleading predictions[46] yielding 17 bona-fide ARC candidate clusters. ARC clusters with at least 25% of cells expressing *Pnoc* were defined as $PNOC^{ARC}$ clusters, additionally we included AgRP neurons, which express *Pnoc* only in a subset of ~10% of cells. For calculating the total percentage of PNOC-expressing cells, cells from the 10 non- ARC PNOC clusters were included as 'others'. Up to 5 marker genes per PNOC cluster were selected using the published marker gene sets filtered for an adjusted p-value < 1e-10, a specificity score > 2.5 and an expression percentage > 25% in the cluster of interest. For the overview of conserved human PNOC neurons, we used data from our published human reference atlas HYPOMAP[22] and the cross-species cluster comparison available from there. We restricted the analysis to the highest correlated cluster for each mouse ARC PNOC cluster (where available) and calculated the percentage of PNOC expression and total percentage of PNOC-expressing cells analogously to the analysis in mouse. Visualization was conducted using functions from the Seurat (v5.0.1), ggplot2 (v3.4.4), schex (v1.16.1) and ggtree (v3.10.0) R packages.

Leptin-stimulated pSTAT3 and immunohistochemistry

Mice received an IP injection of recombinant murine leptin (6 mg/kg body weight; PeproTech; Thermo Scientific, Cat# AF-450-31) dissolved in Phosphate-buffered Saline (PBS) after a 16h overnight fast. Mice were deeply anesthetized 0, 45 or 60 min after leptin injections and transcardially perfused first with ice-cold PBS followed by 2% (w/v) paraformaldehyde (PFA in PBS, pH 7.4). Brains

were post-fixed in 2% PFA in PBS at 4 °C for 4h, then the PFA was replaced with 20% (w/v) sucrose in PBS for 24h before freezing the samples. 20-30 μm brain sections were cut using a cryostat and further processed for pSTAT3 and GFP immunoreactivity. Sections were first post-fixed in 2% PFA for 45–60 min, then incubated with 0.2% NaOH+0.3% H_2O_2 for 20 min, followed by 0.3% Glycine for 10 min and then 0.03% Glycine, all in KPBS buffer. Between each step, slides were washed 3x 10 min in KPBS. Sections were then incubated for 30 min in 4% goat serum+0.3% TritonX (in KPBS) and for 48 h at 4 °C in primary antibody targeting pSTAT3 (#9131, 1:1000, Rabbit, Cell signaling) and/or GFP (#13970, 1:1000, Chicken, Abcam) in blocking buffer. Sections were then washed in KPBS (3 × 10 min) and incubated for 2h with secondary antibody (#A11012, anti-rabbit IgG (goat) Alexa 594, 1:500) and or antibody (103-095155, anti-chicken IgG (goat), FITC 1:500, Jackson) and 1:1000 Dapi. Finally, sections were washed 3x10 min in KPBS before they were mounted with Vectashield (Vector Laboratories Inc., Cat# H1000).

AAV-based NPY expression and immunohistochemistry

Random fed mice were deeply anesthetized and transcardially perfused first with ice-cold PBS followed by 4% (w/v) paraformaldehyde (PFA in PBS, pH 7.4). Brains were post-fixed in 4% PFA in PBS at 4 °C over night, then the PFA was replaced with 20% (w/v) sucrose in PBS for 24h before freezing the samples. 20-30 μm brain sections were cut using a cryostat. Slides were washed with 0,1M PBS containing 0.1% Triton X-100 (PBST) (3x 10 min), then blocked for 60 min at room temperature (PBST, 3% donkey serum). After blocking slides were incubated in primary antibody solution (Rabbit-anti-NPY, 1:1000, Cell-Signaling Technology, and mCherry-monoclonal, 1:1000, Invitrogen in SignalStain® Antibody Diluent, Cell-Signaling Technology) overnight at 4°C. Next, slides were washed with PBST at room temperature (3x 10 min) and incubated in secondary antibody solution (Alexa 647 donkey anti-rabbit, 1:500, Invitrogen, and Alexa 594 donkey anti-rat, 1:500, Invitrogen in SignalStain® Antibody Diluent, Cell-Signaling Technology) for 60 min followed by washing with PBST (3x 10 min). Sections were then mounted with DAPI using Vectashield Antifade Mounting Medium (Vector Laboratories), covered using a coverslip and stored at 4°C in the dark.

RNA *in situ* hybridization

Mouse

Deeply anaesthetized mice were perfused transcardially with ice cold phosphate-buffered saline (pH 7.4) followed by ice cold 4% paraformaldehyde (PFA) dissolved in phosphate-buffered saline (pH 7.4). The brain was removed from the skull and post-fixed in 4% PFA at 4% overnight, and then moved to 20% sucrose solution (in 1X PBS) at 4°C. 20 μm thick sections were cut from frozen tissue using a cryostat. Fluorescent *in situ* hybridization (RNAscope, Advanced Cell Diagnostics) was performed according to the manufacturer's instructions using probes specific for *Pnoc*, *Lepr-Tv1*, *Htr3b*, *Crabp1*, *Sst*, *Satbt, Chst9, Agrp, Npy*, *Egfp, cFos*, together with Opal Flurophores 520/570,650 and 690 *(Akoya Bioscience)*. Sections were mounted on SuperFrost Plus Gold slides (ThermoFisher), dried at RT, briefly rinsed in autoclaved Millipore water, air-dried and incubated at 60°C overnight. Afterward, slides were submerged in Target Retrieval (Cat No. 322000) at 95-99°C for 8 min, followed by a brief rinse in autoclaved Millipore water and dehydrated in 100% ethanol. A hydrophobic barrier was then created around the sections using an ImmEdge hydrophobic barrier pen (Cat No. 310018). Sections were incubated with Protease+ for 15 min. The following hybridization, amplification and detection steps were performed according to the manufacturer's instructions (Multiplex Fluorescent Detection kit v2, Cat No. 323110). Sections were cover slipped and counterstained with DAPI with Vectashield Antifade Mounting Medium (Vector Laboratories) and stored at 4°C in the dark. BaseScope *in situ* hybridization was performed according to the manufacturer's protocol for BaseScope Kit v2-RED (Advanced Cell Diagnostics) using probes specific for *Pnoc* and *Lepr* (deleted region). Sections were dried at 60 °C for 3h, submerged in Target Retrieval reagent at 95-99 °C for 5 min, rinsed in autoclaved Millipore water and dehydrated in 100% ethanol. The following day, sections were incubated with Protease III (Cat# 322340) for 30 min at 40 °C. Amplification and detection steps were performed according to the manufacturer's protocol. Sections were counterstained with Haematoxylin and cover-slipped.

Human

Tissue blocks covering mediobasal hypothalamus were obtained from the Edinburgh Brain Bank (n=3, 2M+1F: BBN001.37298, BBN001.37137, BBN001.37273) in collaboration with Professor Colin Smith, following UK and DK legal and ethical guidelines. Fluorescent in situ hybridization (FISH) was performed on formalin fixed paraffin embedded human brain blocks covering the mediobasal hypothalamus. The tissue blocks was sectioned at 5 μm and mounted onto Fisher SuperFrost Plus glass slides (Fisher Scientific). Multiplex FISH was performed using the RNAscope LS multiplex fluorescent reagent kit and RNAscope LS 4-Plex Ancillary Kit Multiplex Reagent Kit (Advanced Cell Diagnostics, Bio-Techne, Cat #322800+#322830) together with iFluor488/iFluor546/iFlour594 (1:500, AAT Bioquest/VWR, Cat #45020/45025/45035) and Opal690 Fluorophore Reagent pack detection (1:500, Cat #FP1497001KT, Akoya Biosciences) on a Leica BOND RX Fully Automated Research Stainer (Leica Biosystems) according to the manufacturer's instructions. The human tissue sections were pre-treated for 30 min with HIER at 95°C in ER2 followed by 15 min protease treatment and then hybridized with human-specific probes to detect mRNA transcripts for *AGRP* (#557458), *LEPR-TV1* (long isoform, #410378-C2), *NPY* (#416678-C3) and *PNOC* (#1045248-C4) (Advanced Cell Diagnostics, Bio-Techne). As positive and negative controls, ACD 4-plex Multiplex Positive and Negative Control Mixes (Cat #321808 and #321838, ACD/Biotechne) was used. Slides were counterstained with DAPI and then cover slipped with Prolong TM Gold Antifade mountant (ThermoFisher Scientific).

Please cite this article in press as: Solheim et al., Hypothalamic PNOC/NPY neurons constitute mediators of leptin-controlled energy homeostasis, Cell (2025), https://doi.org/10.1016/j.cell.2025.04.001

Imaging and quantifications

Mouse

Brightfield images were acquired on an Axio Imager 2 microscope operated by ZEN 2 (blue edition) software using an Axiocam 105 color camera (Carl Zeiss Microscopy GmbH). Confocal images for quantifications were obtained from two separate brain slices per mouse using a Leica TCS SP-8-X or Stellaris 8 confocal microscope equipped with x40/1.30 oil objective. If two good sections were not found, more animals were used in the analysis. Tile scans were automatically assembled by the LasX software. The same microscope settings for the detection (including objective, zoom, laser power, gain) were used to acquire all pictures of the same experiment. For quantification and image representation, maximum intensity projections of z-stacks were produced using the Fiji software or Imaris image analysis software. Regions of interest were manually drawn based on anatomical landmarks. Images were quantified using the Imaris image analysis software applying identical quantification thresholds for all samples. Immunostainings of pSTAT3/GFP and Basescope sections were counted manually. Signal intensity levels were adjusted to match across slides.

Human

Fluorescent slide scans were acquired with an Olympus VS200 slide scanner (Olympus) using a 20x (0.8 NA) air objective and 385/470;488/520;546/570;594/620 filter sets. Quantification of *PNOC/NPY/AGRP* ISH positive cells were performed using the FISH v3.2.3 module in image analysis software HALO (Indica Labs), applying identical quantification thresholds for all samples. Regions of interest for ARC were manually drawn based on anatomical landmarks. Images were prepared with the HALO software, and signal intensity levels were adjusted to match across slides.

Statistics

All data are represented as mean ±SEM. Graphpad Prism software (version 10) was used to perform the statistical analysis. To compare two independent groups, unpaired two-tailed Student's t test was performed. Datasets consisting of more than two groups were analyzed using one-way analysis of variance (ANOVA) followed by Tukey's or Dunnett's post hoc multiple comparison test. Longitudinal data were analyzed using two-way repeated-measures (RM) ANOVA with Geisser-Greenhouse correction. A p value of 0.05 was considered significant.

CellPress
OPEN ACCESS

Supplemental figures

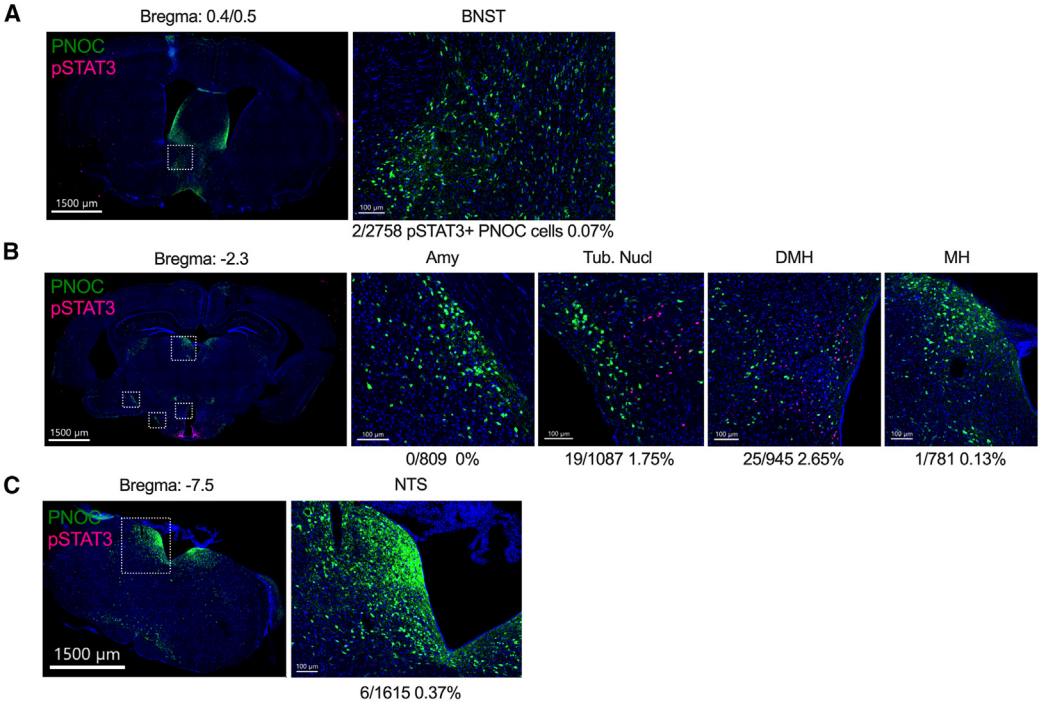

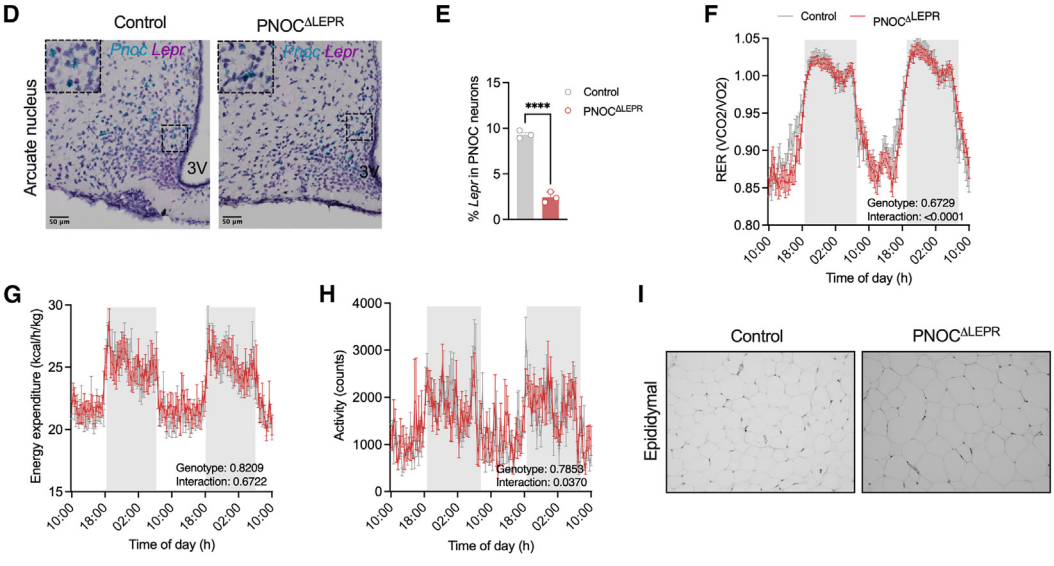

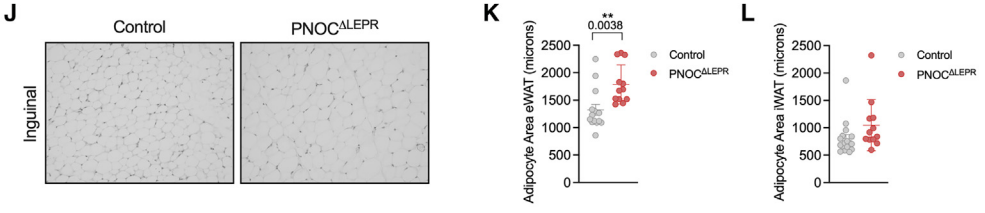

(legend on next page)

Figure S1. Leptin-induced pSTAT3-signaling in PNOC neurons is limited to the ARC and Cre-mediated recombination, inducing metabolic dysfunction in PNOC$^{\Delta LEPR}$ animals, related to Figure 1

(A–C) Confocal images of brain sections of PNOC-EGFP mice fasted for 16 h and immunolabeled for pSTAT3 (magenta) and EGFP (green) 60 min post leptin injection (6 mg/kg), displaying (A) brain section from bregma 0.4/0.5, including the bed nucleus of the stria terminalis (BNST), (B) bregma −2.3 covering the Amy, lateral tuberal nucleus (Tub. Nucl), dorsal medial hypothalamus (DMH), medial habenula (MH), and (C) bregma −7.5, including the nucleus of the solitary tract (NTS). Number of cells counted and percent pSTAT3+ PNOC cells is indicated below each region. Scale bars 1500 μm, 100 μm (zoom)

(D and E) (D) Bright-field images of BaseScope *in situ* hybridization on brain sections from LEPR-Flox control and PNOC$^{\Delta LEPR}$ mice using a probe targeting the *Pnoc* transcript (blue), together with a probe targeting exon 1 in the *Lepr* transcript (deleted exon) (magenta) in brain sections from control and PNOC$^{\Delta LEPR}$ mice, and the (E) quantification of percent *Lepr*-positive PNOC cells in the ARC (n = 3/each group). Scale bars 50 μm.

(F–L) (F) Respiratory exchange ratio (RER), (G) EE, and (H) activity levels of male LEPR-Flox control (gray) and PNOC$^{\Delta LEPR}$ animals (red) (n = 12 vs. 12 mice) at 15–16 weeks of age (gray area indicates dark/night phase). Bright-field images of hematoxylin- and eosin-stained (I) epididymal and (J) inguinal formalin fixed fat sections at 20 weeks of age and (K and L) adipocyte area quantified using ImageJ (Adiposoft plugin). Data are represented as mean ± SEM. Male animals, (n = 17 vs. 12) p values calculated using two-way RM ANOVA (F–H) or two-tailed unpaired Student's t test (E, K, and L). **p ≤ 0.01; ****p ≤ 0.0001.

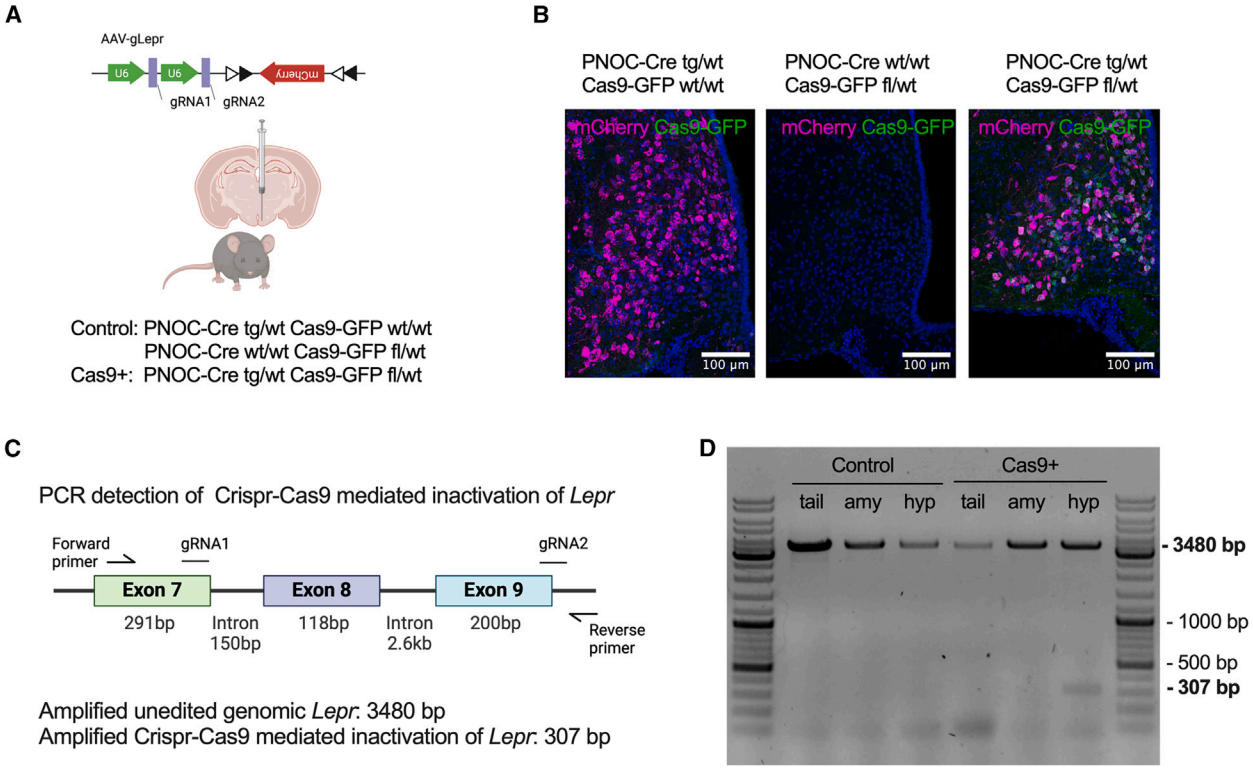

(legend on next page)

Figure S2. Ablating LEPRs in the PNOC ARC neurons promotes hyperphagia and obesity, related to Figure 1

(A) Schematic of the CRISPR-Cas9 KO strategy to ablate *Lepr* in PNOC cells. Rosa26-Cas9-EGFP mice were bred with PNOC-Cre mice, creating a Cas9+ PNOC-Cre Tg/WT and Cas9-GFP Fl/WT mice (green). The control group included littermate Pnoc-Cre WT/WT and Cas9-GFP Fl/WT animals, as well as Pnoc-Cre Tg/WT and Cas9-GFP WT/WT animals (gray). All animals received stereotactic delivery of an AAV for expression of the *Lepr* guideRNA (gRNA) as well as Cre-dependent expression of *mCherry*.

(B) Confocal images depicting PNOC-neuron-restricted Cre-dependent expression of mCherry from the AAV-gRNA vector and Cre-dependent expression of eGFP in PNOC-Cre::Cas9-GFP mice. All animals received stereotactic ARC delivery of AAV-gRNA (*Lepr*) (mCherry, magenta); Cas9-GFP is shown in green. Scale bars 100 μm.

(C and D) (C) Scheme depicting PCR strategy to detect CRISPR-Cas9-mediated inactivation of the *Lepr* (a PCR-amplified region of 307 bp) and (D) image of agarose gel depicting a PCR-amplified *Lepr* region flanking the genome-edited region on DNA isolated from tail, Amy, and hypothalamus biopsies of control and Cas9+ animals.

(E and F) (E) Percent weight gain of control and Cas9+ animals, 5 weeks post AAV delivery, and (F) body composition measured by uCT.

(G–I) (G) Cumulative food intake over the indicated time, (H) RER, and (I) EE 4 weeks post injection. Data are represented as mean ± SEM, n = 10–11. p values calculated using two-tailed unpaired Student's t test (E and F) or two-way RM ANOVA (G–I). **p $\leq$ 0.01; ***p $\leq$ 0.001.

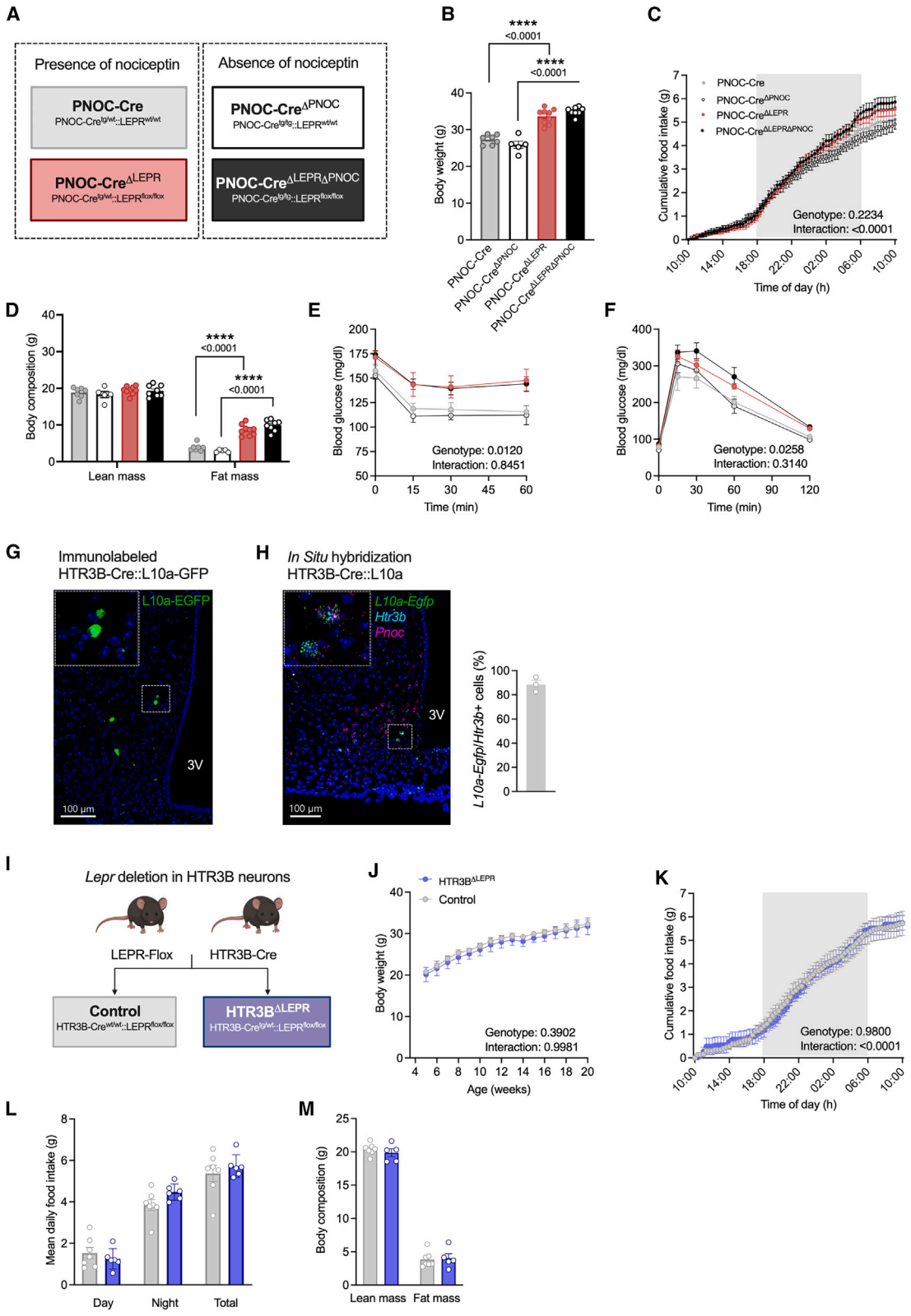

(legend on next page)

Figure S3. Hyperphagia due to PNOC LEPR deletion is independent of PNOC expression, and the absence of LEPR in HTR3B neurons does not change food intake or body weight, related to Figures 1 and 3

(A) Schematic showing four study groups designed to determine the role of nociceptin expression upon *Lepr* inactivation in PNOC cells: two groups with *Pnoc* expression; PNOC-Cre (gray) and PNOC-Cre$^{\Delta LEPR}$ (red) and two groups with inactivated *Pnoc* expression; PNOC-Cre$^{\Delta PNOC}$ (white) and PNOC-Cre$^{\Delta LEPR\Delta PNOC}$ (black) resulting from intercrossing of either PNOC$^{\Delta LEPR}$ mice or PNOC-Cre mice.

(B–D) (B) Body weights of male mice at 15–16 weeks of age from all four groups, and (C) the cumulative food intake over the indicated time, followed by (D) body composition measured by uCT.

(E and F) (E) Insulin and (F) glucose tolerance tests from all four groups (n = 5 vs. 9 mice).

(G and H) (G) Immunostaining of brain sections from HTR3B-Cre::L10A animals, showing L10a-GFP-marked HTR3B (green) and (H) *in situ* hybridization showing co-localization of *Pnoc* (magenta), *Htr3b* (cyan), and *Egfp* (L10a, green) quantifying percent *L10a-EGFP*/*Htr3b*+ cells (n = 3). Scale bars 100 μm.

(I) Schematic of the KO strategy used to inactivate LEPR in HTR3B cells. LEPR-Flox mice were bred with mice carrying transgenic Cre-expression under the control of the HTR3B promoter.

(J) Weekly body weight progression in male LEPR-Flox control (gray) and HTR3B$^{\Delta LEPR}$ animals (blue) measured over the indicated time course (n = 8 vs. 6 mice).

(K–M) (K) Cumulative food intake across the day, (L) mean daily food intake shown as average of 2 consecutive day and (M) micro-CT analysis of lean and fat mass at 16 weeks of age. Data are represented as mean ± SEM. p values calculated using one-way ANOVA followed by Tukey's multiple comparison test (B and D), two-way RM ANOVA (C, E, F, J, and K), or (L and M) two-tailed unpaired Student's t test. ****$p \leq 0.0001$.

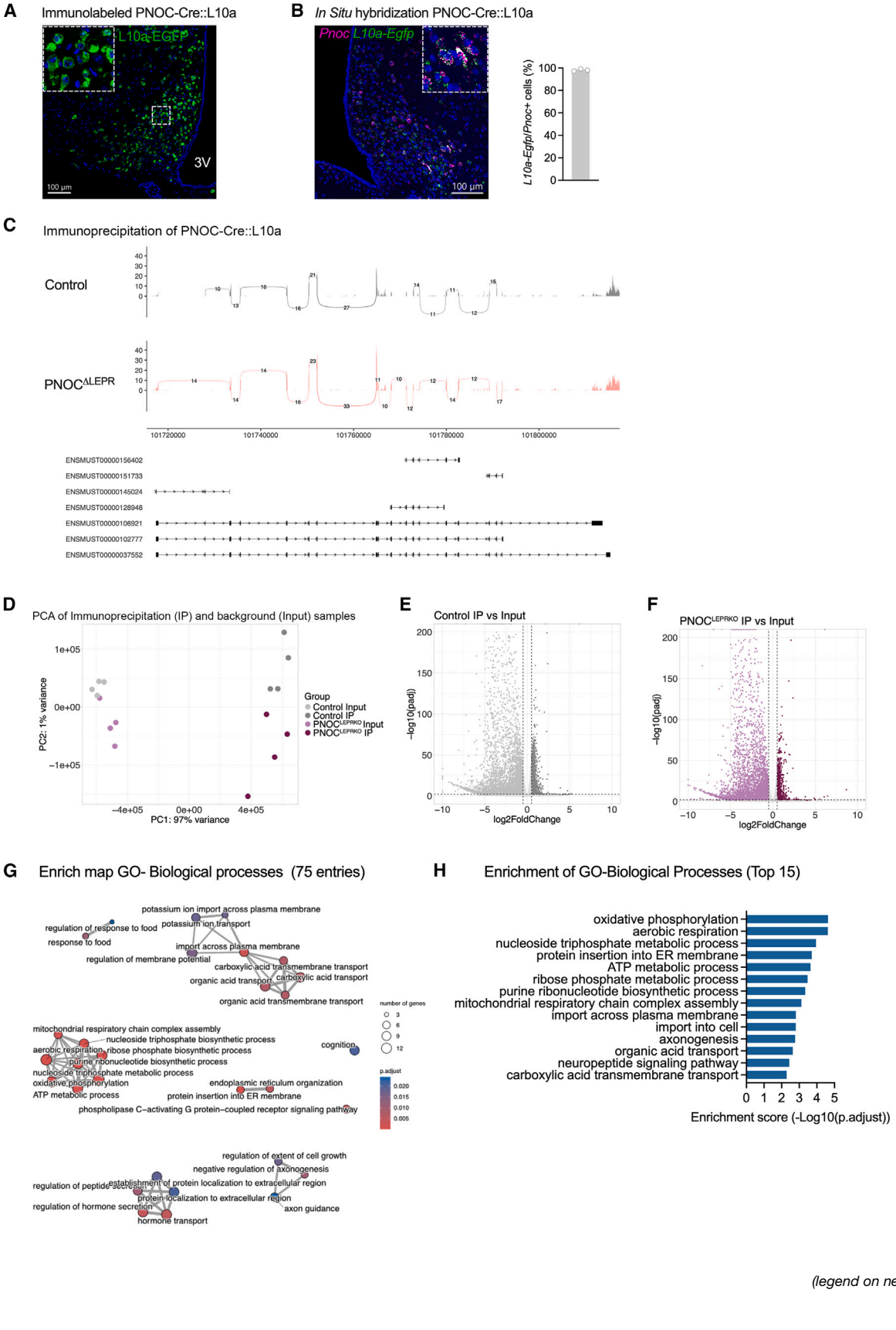

(legend on next page)

Figure S4. Validation of PNOC-neuron-restricted L10a-GFP ribosome tagging and ribosome profiling of PNOC neurons in control and PNOC$^{\Delta LEPR}$ animals, related to Figure 4

(A and B) (A) Immunostaining of brain sections from PNOC-Cre::L10A animals, showing L10a-GFP marked PNOC neurons (green) and (B) *in situ* hybridization showing co-localization of *Pnoc* (magenta) and *Egfp* (L10a, green), quantifying the percentage of L10a-EGFP/PNOC+ cells (n = 3). Scale bars 100 μm.

(C) ggSashimi visualization of splicing events and read coverage of the *Lepr* gene by displaying exon-spanning reads in hypothalamic samples following pull-down in control (gray) and PNOC$^{\Delta LEPR}$ (magenta). For visual clarity, we require a minimum of 10 exon-spanning reads to be displayed. The plots show a splicing event in exon 1 (or exon 2 if counting the first untranslated exon) of the PNOC$^{\Delta LEPR}$ condition as well as a lower read coverage compared with control.

(D–F) (D) PCA plot of hypothalamic bacTRAP pull-down (IP) and background (input) samples of control and PNOC$^{\Delta LEPR}$ mice; (E) volcano plot displaying differentially expressed genes between IP and input in control animals and (F) PNOC$^{\Delta LEPR}$ animals.

(G and H) (G) GO enrichment analysis revealed upregulated biological processes between control and PNOC$^{\Delta LEPR}$ mice, shown as enrichment map (75 entries), and (H) enrichment of the top 15 biological processes.

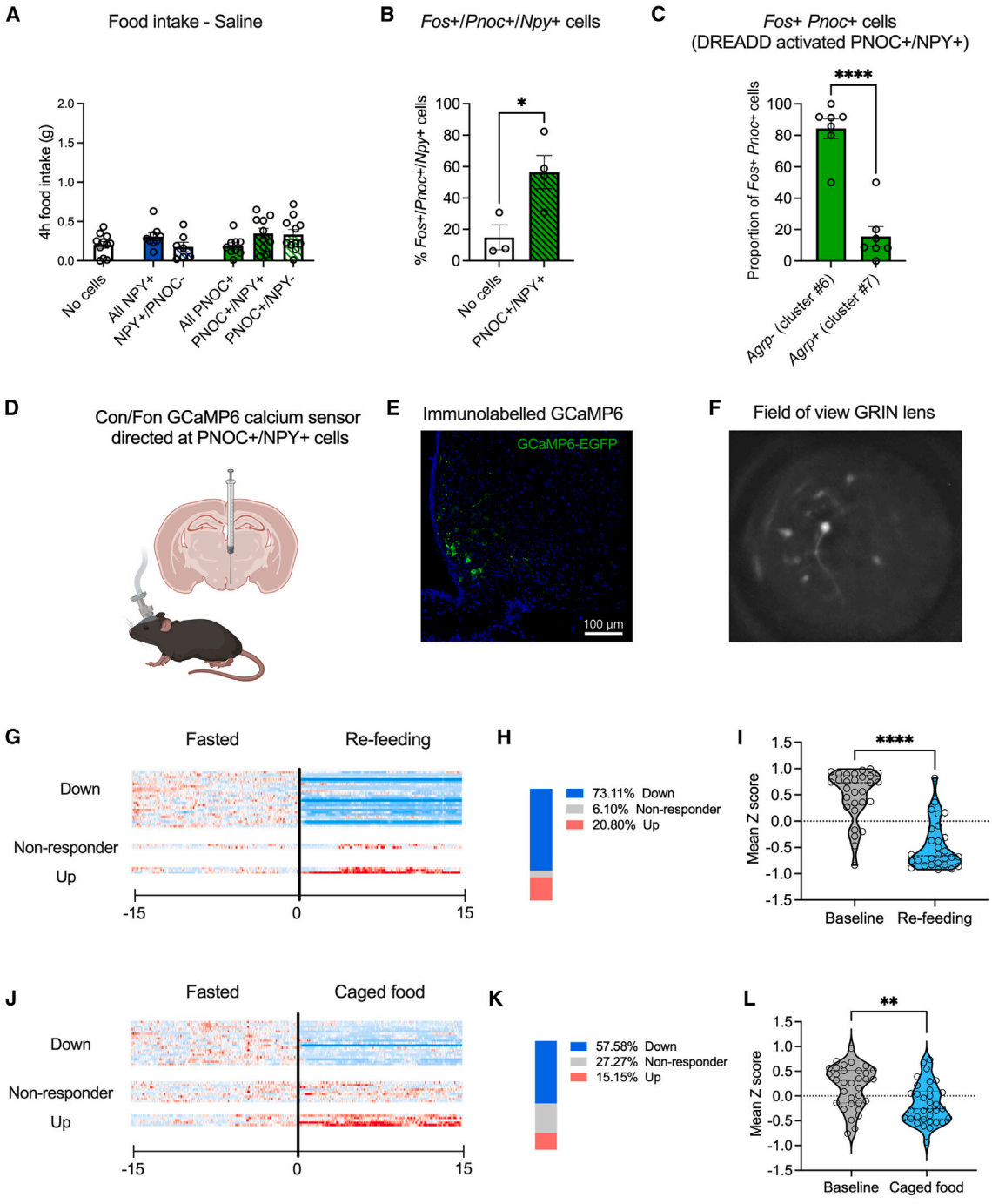

Figure S5. DREADD activation of PNOC+/NPY+ cells predominantly activates AgRP-negative cluster #6 PNOC ARC neurons, and single-cell calcium imaging shows that they are inhibited upon feeding, related to Figure 5

(A) Food intake 4 h following saline treatment (morning, 8 a.m.) of all groups.

(B and C) (B) Quantification of percent *Fos+/Pnoc+/Npy+* cells from *in situ* hybridization RNAscope performed on brain sections from CNO-activated (1 mg/kg, 1 h) PNOC+/NPY+-targeted cells and (C) proportion of *Agrp+* or *Agrp− Fos+/Pnoc+* cells in the same group. *p* values calculated using one-way ANOVA followed by Tukey's multiple comparison test (A) or two-tailed unpaired Student's t test (B and C). *p ≤ 0.05; ****p ≤ 0.0001.

(D) Schematic of unilateral delivery of an intersectional Cre-on/Flp-on GCaMP6 calcium sensor into the ARC of Pnoc-Cre::NPY-Flp animals, followed by GRIN lens implantation directly above ARC.

(E and F) (E) Immunolabeled GCaMP6s (GFP) in PNOC-Cre::NPY-Flp, targeting PNOC/NPY cells (green), and (F) mini-scope field of neuronal view at lens depth. Scale bar 100 µm.

(legend continued on next page)

(G) Heatmap showing recordings of each individual neuron (29 neurons total), 15 min baseline-fasted condition and 15 min following re-feeding.
(H) Each neuron was normalized to its own baseline (*Z* score) and partitioned into three groups using k-medoids clustering. Graph indicating in blue the percentage of neurons considered inhibited (down), non-responders (gray), and in red activated neurons (up).
(I) Mean *Z* score of baseline recording and recording following re-feeding.
(J–L) (J) Heatmap showing all individual neurons (33 neurons) in animals receiving a caged non-consumable food pellet; (K) percentage of neurons considered inhibited, activated, or non-responding; and (L) mean *Z* score of baseline and after caged food presentation.

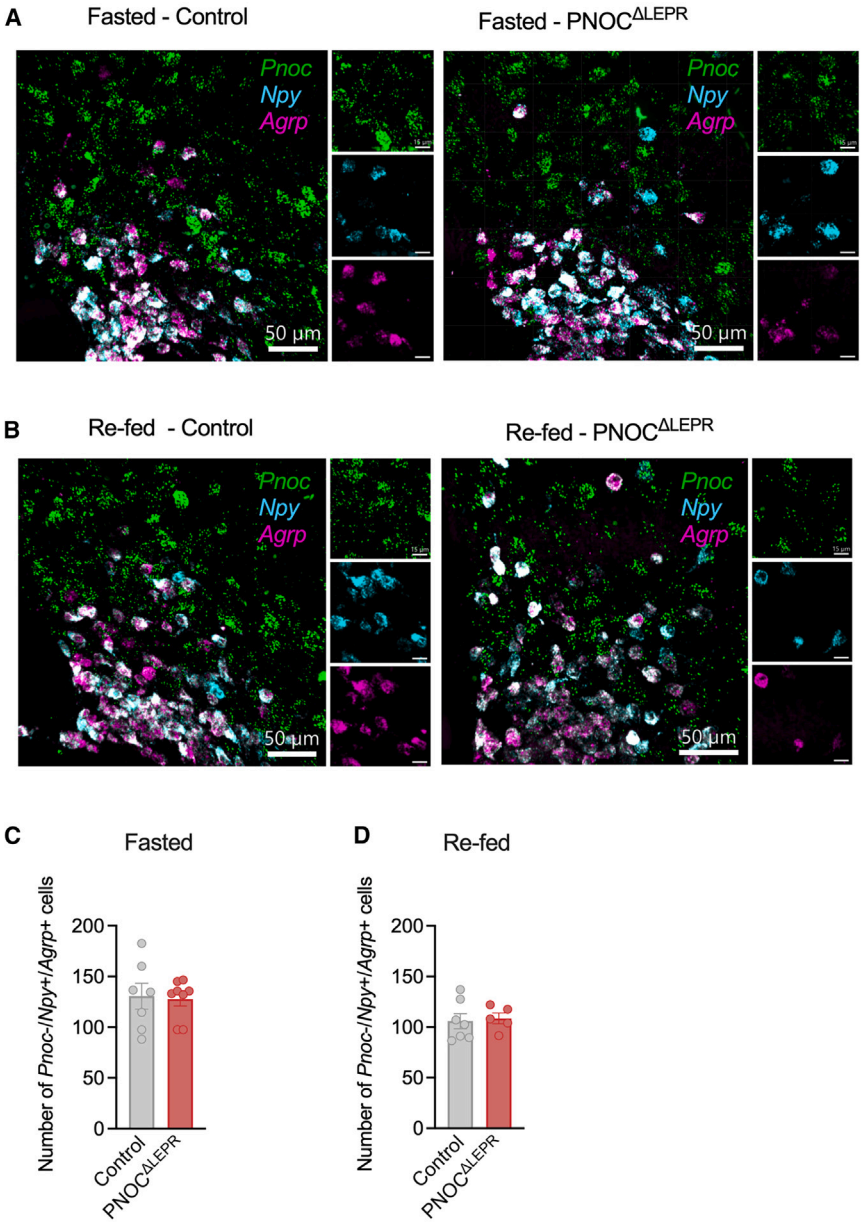

Figure S6. Increased NPY expression in PNOC neurons of PNOC$^{\Delta LEPR}$ mice, but not in AgRP neurons, related to Figure 6

(A and B) Representative confocal images showing *in situ* hybridization mRNA expression of *Pnoc* (green), *Npy* (cyan), and Agrp (magenta) in (A) fasted control and PNOC$^{\Delta LEPR}$ animals and (B) re-fed animals. Scale bars 50 µm, 15 µm (zoom).

(C and D) (C) Number of NPY+/AgRP+ cells quantified from the *in situ* hybridization analysis in 16-h-fasted conditions and (D) 1 h re-feeding following 16 h fasting. Data are represented as mean ± SEM. *p* values calculated using two-tailed unpaired Student's t test, *n* = 5–7 animals, 2 sections each.

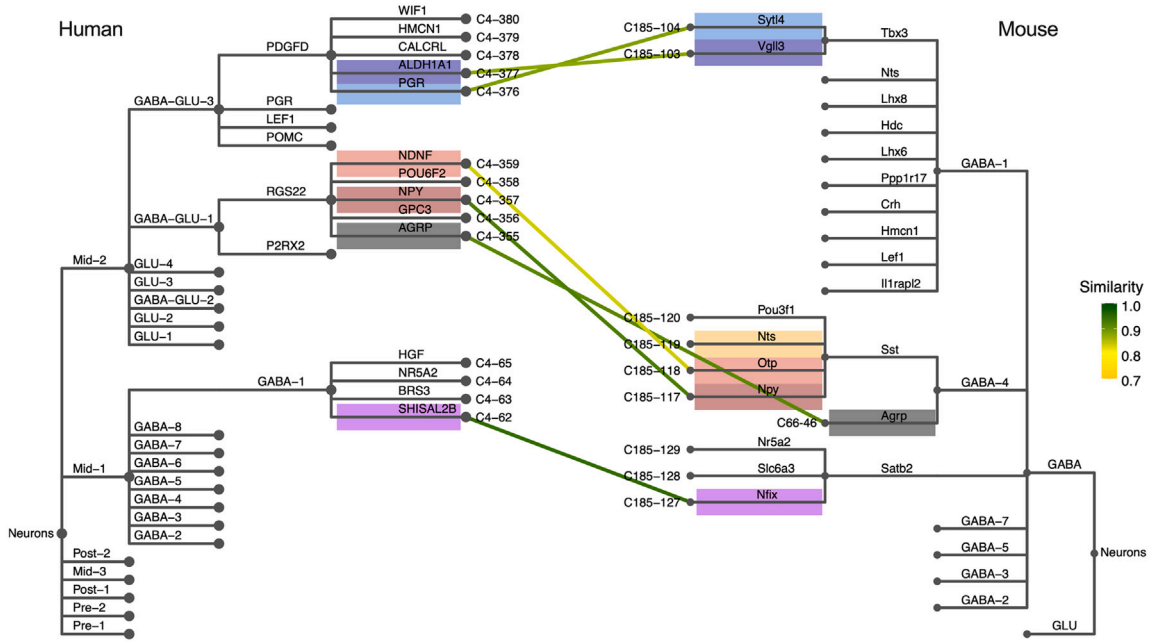

Figure S7. Comparison of human and murine PNOC^{ARC} neuron clusters, related to Figures 3 and 7

Left: dendrogram of human HYPOMAP neuronal clusters. Right: dendrogram of corresponding mouse HypoMap clusters. PNOC^{ARC} clusters are highlighted in colors corresponding to Figures 3A, 3B, and 7A. Edges of dendrograms are annotated with cluster names from human and mouse HypoMap, and only PNOC^{ARC} neurons and their closest-related clusters are displayed with full names and identifier. Line color depicts correlation between clusters.